Remote Sensing of Environment 211 (2018) 425–440

Contents lists available at ScienceDirect

Remote Sensing of Environment

journal homepage: www.elsevier.com/locate/rse

Mapping soil moisture with the OPtical TRApezoid Model (OPTRAM) based on long-term MODIS observations

Ebrahim Babaeian[a,*], Morteza Sadeghi[b], Trenton E. Franz[c], Scott Jones[b], Markus Tuller[a]

[a] Dept. Soil, Water and Environmental Science, The University of Arizona, Tucson, AZ, USA
[b] Dept. Plants, Soils and Climate, Utah State University, Logan, UT, USA
[c] School of Natural Resources, University of Nebraska-Lincoln, Lincoln, NE, USA

ARTICLE INFO

Keywords:
Soil moisture mapping
The OPtical TRApezoid Model (OPTRAM)
Drought monitoring
Cosmic-ray neutron soil moisture
MODIS
SMAP
SMOS
ASCAT

ABSTRACT

The OPtical TRApezoid Model (OPTRAM) has recently been proposed for estimation of soil moisture using only optical remote sensing data. The model relies on a physical linear relationship between the soil moisture content and shortwave infrared transformed reflectance (STR) and can be parameterized universally (i.e., a single calibration for a given area) based on the pixel distribution within the STR-Normalized Difference Vegetation Index (NDVI) trapezoidal space. The main motivation for this study was to evaluate how the universal parameterization of OPTRAM works for long periods of time (e.g., several decades). This is especially relevant for uncovering the soil moisture and agricultural drought history in response to climate change in different regions. In this study, MODIS satellite observations from 2001 to 2017 were acquired and used for the analysis. Cosmic-ray neutron (CRN) soil moisture data, collected with the COsmic-ray Soil Moisture Observing System (COSMOS) at five different sites in the U.S. covering diverse climates, soil types, and land covers, were applied for evaluation of the MODIS-OPTRAM-based soil moisture estimates. The OPTRAM soil moisture estimates were further compared to the Soil Moisture Active and Passive (SMAP) (L-band), the Soil Moisture Ocean Salinity (SMOS) (L-band), and the Advanced AScatterometer (ASCAT) (C-band) soil moisture retrievals. OPTRAM soil moisture data were also analyzed for potential monitoring of agricultural drought through comparison of the OPTRAM-based Soil Water Deficit Index (OPTRAM-SWDI) with the widely-applied Crop Moisture Index (CMI). Evaluation results indicate that OPTRAM-based soil moisture estimates provide overall unbiased *RMSE* and *R* between 0.050 and 0.085 $cm^3\,cm^{-3}$ and 0.10 to 0.70, respectively, for all investigated sites. The performance of OPTRAM is comparable with the ASCAT retrievals, but slightly less accurate than SMAP and SMOS. OPTRAM and the three microvave satellites captured CRN soil moisture temporal dynamics very well for all five investigated sites. A close agreement was observed between the OPTRAM-SWDI and CMI drought indices for most selected sites. In conclusion, OPTRAM can estimate temporal soil moisture dynamics with reasonable accuracy for a range of climatic conditions (semi-arid to humid), soil types, and land covers, and can potentially be applied for agricultural drought monitoring.

1. Introduction

Soil moisture is a highly dynamic state variable that controls fundamental hydrological processes such as evaporation, infiltration, and runoff. It is also critical for management and allocation of water resources, prediction and monitoring of drought, agricultural production, mitigation of natural disasters and monitoring of ecosystem response to climate change (Robinson et al., 2008; Vereecken et al., 2014; Babaeian et al., 2016).

Remote sensing techniques provide powerful means for characterizing and monitoring the high spatiotemporal variability of soil moisture. During the past decade, several satellites with various spatiotemporal resolutions have been launched for monitoring near surface (0–5 cm) soil moisture, including the European Soil Moisture and Ocean Salinity (SMOS) Satellite, launched in 2009 (Kerr et al., 2001), the Advanced Microwave Scanning Radiometer 2 (AMSR-2) on the Global Change Observation Mission-Water (GCOM-W1) Satellite, launched in 2012, the Advanced Scatterometer (ASCAT) launched in 2006 on the EUMETSAT MetOp-A and MetOp-B satellites, the ESA Sentinel-1 Satellite launched in 2014 (Bartalis et al., 2007), and NASA's Soil Moisture Active-Passive (SMAP) Satellite, launched in 2015 (Entekhabi et al., 2010). These microwave satellites yield the most accurate

* Corresponding author at: 1177 E. 4th Street, Tucson, AZ 85721, USA.
E-mail addresses: ebabaeian@email.arizona.edu (E. Babaeian), morteza.sadeghi@usu.edu (M. Sadeghi), tfranz2@unl.edu (T.E. Franz), scott.jones@usu.edu (S. Jones), mtuller@email.arizona.edu (M. Tuller).

https://doi.org/10.1016/j.rse.2018.04.029
Received 9 December 2017; Received in revised form 19 March 2018; Accepted 13 April 2018
Available online 25 April 2018
0034-4257/

measurements of soil moisture (Mattikalli et al., 1998) because of the high dielectric permittivity of soil water within the microwave domain (Hallikainen et al., 1985) and the greater penetration of microwaves through vegetation canopy and underlying soil (Escorihuela et al., 2010; Chapin et al., 2012; Tabatabaeenejad et al., 2015).

Passive microwave satellites commonly provide high temporal resolution observations (e.g., daily), but suffer from low spatial resolution. Within this context, optical and thermal remote sensing observations provide higher spatial resolution information and thus are often used to enhance the passive microwave soil moisture maps through data fusion and downscaling approaches (e.g., Piles et al., 2014; Merlin et al., 2012). Hence, development of robust optical and thermal methods, in concert with microwave techniques, can improve remote sensing of soil moisture.

The trapezoid (or triangle) model is a widely-applied approach to remote sensing of soil moisture based on thermal (land surface temperature, *LST*) and optical data (Carlson et al., 1994; Gillies and Carlson, 1995; Owen et al., 1998; Rahimzadeh-Bajgiran et al., 2013; Shafian and Maas, 2015; Sun, 2016). Despite the trapezoid model's obvious success discussed in Sadeghi et al. (2017), it suffers from two inherent limitations. The first is the requirement of concurrent optical and thermal data, which renders the model inapplicable to satellites that do not provide thermal data (e.g., ESA Sentinel-2). The second limitation is that the land surface temperature is not only affected by soil moisture content but also by ambient atmospheric conditions (e.g., wind speed, air temperature, and air humidity). Hence, the conventional trapezoid model needs time consuming and computationally demanding individual parameterization (calibration) for each individual observation date. To overcome these two limitations, Sadeghi et al. (2017) proposed the physically-based OPtical TRApezoid Model (OPTRAM) for estimation of surface soil moisture. The OPTRAM trapezoid is formed by distribution of the normalized difference vegetation index (NDVI) as a measure of vegetation fraction versus shortwave-infrared (SWIR) transformed reflectance to obtain soil moisture content. This concept was introduced by Sadeghi et al. (2015). The OPTRAM does not require a thermal band, hence, it is applicable to satellites providing optical bands only (this resolves the first limitation of the conventional trapezoid model). Because SWIR reflectance does not significantly change with ambient atmospheric conditions, OPTRAM can be universally parameterized for a given location (this resolves the second limitation of the conventional trapezoid model).

OPTRAM has been initially evaluated in Sadeghi et al. (2017) based on ESA Sentinel-2 and NASA Landsat-8 satellite observations for mapping of soil moisture in the Walnut Gulch and Little Washita watersheds in Arizona and Oklahoma, respectively. Because Sentinel-2 was only recently launched (i.e., in summer 2015), the time period covered in the Sadeghi et al. (2017) study was limited to a few months in 2015 and 2016. Hence, the main motivation for this current study was to evaluate how the universal parameterization of OPTRAM (i.e., a single calibration for a given area) works for long periods of time (e.g., several decades). This is especially important with regard to expanding our ability to uncover the soil moisture history in response to climate change in different regions.

Long-term soil moisture data provide a useful measure for monitoring agricultural drought (Chakrabarti et al., 2014), which is defined based on the soil water deficit and its effects on crop production. Recently, several studies have shown the potential of remotely sensed soil moisture data for agricultural drought monitoring (Chakrabarti et al., 2014; Martinez-Fernandez et al., 2016; Carrao et al., 2016; Mishra et al., 2017; Liu et al., 2017). Several soil moisture-based drought indices have also been introduced for agricultural drought monitoring including the Soil Moisture Index (SMI) (Sridhar et al., 2008), Soil Water Deficit (SWD) (Torres-Ruiz et al., 2013), Plant Available Water (PAW) (McPherson et al., 2007), Drought Severity Index (DSI) (Cammalleri et al., 2016), Soil Moisture Drought Index (SMDI) (Sohrabi et al., 2015), and Soil Water Deficit Index (SWDI) (Martinez-Fernandez et al., 2015). Among these drought indices, SWDI is a simple agricultural drought index that is computed based on plant water availability, which is assumed to not change over long time periods. The SWDI has been recently used in conjunction with remotely sensed soil moisture estimates from SMAP and SMOS for monitoring agricultural drought (Martinez-Fernandez et al., 2016; Mishra et al., 2017). The application of microwave-based soil moisture retrievals (e.g., SMAP, SMOS, Sentinel-1) for long-term monitoring of agricultural drought is limited due to the lack of soil moisture data for long periods of time. The optical satellites such as Landsat and MODIS, launched many years before SMAP, SMOS, and Sentinel-1, provide a unique opportunity for such analysis in order to fill this critical observational gap.

The specific objectives of this study were to: (*i*) evaluate the universally-parameterized OPTRAM for estimation of soil moisture with long-term MODIS data for four watersheds in the United States, which exhibit diverse climates, soil types, and land covers, (*ii*) compare the accuracy of OPTRAM soil moisture estimates with retrievals from microwave satellites (i.e., SMAP, SMOS, ASCAT), and (*iii*) explore the feasibility of applying long-term OPTRAM soil moisture data for agricultural drought monitoring.

2. Background: the Optical TRApezoid Model (OPTRAM)

Sadeghi et al. (2017) proposed a physically-based trapezoidal space termed the "OPtical TRApezoid Model" (OPTRAM) for remote sensing of soil moisture based on optical data only. The concept is based on the pixel distribution within the *STR-NDVI* space, where *STR* is the SWIR transformed reflectance and *NDVI* is the normalized difference vegetation index, thereby replacing *LST* in the conventional trapezoid model. Considering a linear relationship between soil saturation degree, *W* (0 for completely dry and 1 for saturated soil) and *STR* (Sadeghi et al., 2015) results in:

$$W = \frac{STR - STR_d}{STR_w - STR_d} \tag{1}$$

where:

$$STR = \frac{(1-R)^2}{2R} \tag{2}$$

where STR_d and STR_w are *STR* at dry (e.g., $\theta \sim 0\ cm^3\ cm^{-3}$, where θ is volumetric moisture content) and wet (e.g., $\theta = \theta_s\ cm^3\ cm^{-3}$, where θ_s is saturated moisture content) states, respectively, and *R* is surface reflectance for the SWIR electromagnetic domain (i.e., 2130 nm, MODIS band 7). Assuming an empirical linear relationships of STR_d and STR_w with vegetation fraction, the dry and wet edges of the optical trapezoid are defined as follows (see Fig. 1):

$$STR_d = i_d + s_d NDVI \tag{3}$$

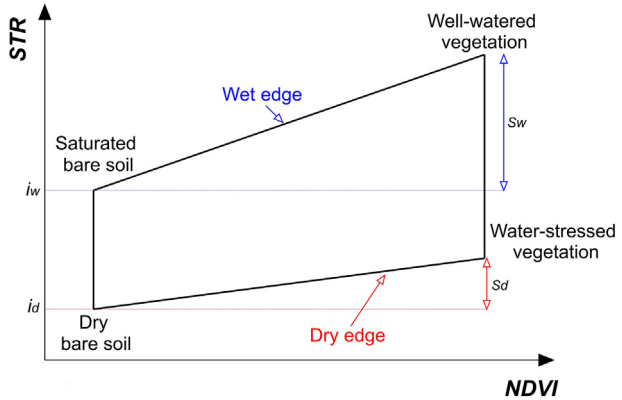

Fig. 1. The OPtical TRApezoid Model (OPTRAM) relating *STR* [Eq. (2)] and *NDVI*.

$$STR_w = i_w + s_w NDVI \quad (4)$$

where i_d and s_d are intercept and slope of the dry edge and i_w and s_w are intercept and slope of the wet edge.

Based on Eqs. (1), (3) and (4), soil moisture within a given satellite image pixel can be estimated from its *STR* and *NDVI* values:

$$W = \frac{i_d + s_d NDVI - STR}{i_d - i_w + (s_d - s_w) NVDI} \quad (5)$$

where the saturation degree W can be expressed as θ ($cm^3\,cm^{-3}$) when multiplied with the soil porosity (assumed equal to θ_s).

As discussed in Sadeghi et al. (2017), unlike the conventional trapezoidal space (*LST* vs. *NDVI*) that varies over time due to variation of the ambient atmospheric parameters, the *STR-NDVI* space is nearly time-invariant because surface reflectance is only dependent on surface properties and not on the ambient atmospheric parameters. Therefore, we hypothesize that a universal parameterization of Eq. (5) is possible with prolonged time series of satellite observations for any specific location.

3. Materials and methods

3.1. Study areas

The OPTRAM was evaluated for four watersheds in the United States with diverse climates, soil types and land covers, where existing cosmic-ray neutron (CRN) soil moisture observations were used as reference for soil moisture data (Fig. 2). Characteristics of the CRN sites within the four watersheds are summarized in Table 1. A brief introduction of these watersheds follows.

3.1.1. Walnut Gulch, Arizona

The Walnut Gulch Watershed (WGW), located in southeastern Arizona (AZ), with an area of 148 km^2 is one of the most intensively instrumented semi-arid rangeland watersheds in the world. It was developed as a research watershed for hydrologic and atmospheric sciences by the United States Department of Agriculture (USDA) in 1953. The watershed has been frequently used as a core validation site for aircraft- and satellite-based remote sensing of soil moisture. The WGW includes two CRN sites: “Lucky Hills” and “Kendal”. They are dominantly covered with desert shrubs (two thirds) and desert grasses (one third). The soils are mostly sandy loam and gravelly loam with little organic matter content. The climate is semi-arid with an average annual temperature of 17.7 °C and an annual average precipitation of 350 mm; about two-thirds commonly falls during the summer monsoon season (July to September). The potential evapotranspiration is approximately ten times the annual precipitation. The topography exhibits gently rolling hills incised by steep drainage channels (Renard et al., 1993; Keefer et al., 2008).

3.1.2. Willow Creek, California

The Willow Creek Watershed (WCW) with an area of 58 km^2 is located East of Sacramento, California (CA). The watershed encompasses the “Tonzi Ranch” CRN site that has been established in a fairly flat area covered with oak-grass savanna. Tonzi Ranch is one of the SMAP validation sites. Sandy clay loam with low organic matter content is the dominant soil texture. The land surface is covered with mixed forests, grasslands and shrublands. The typical land forms consist of plains, shallow valleys, and hills. The elevation ranges from 50 to 450 m above sea level. The climate is Mediterranean with an average annual temperature of 16 °C and an average annual precipitation of 560 mm mostly falling between November and March.

3.1.3. Reynolds Creek, Idaho

The USDA Reynolds Creek Experimental Watershed (RCW), located in Southwestern Idaho (ID), is a key watershed that has been established to support research addressing issues of water quantity and quality, seasonal snow, and rangeland hydrology of the interior Pacific northwest. The RCW is equipped with one CRN station and very well instrumented with neutron access tubes, weirs, fiber optic temperature cables, and snow survey stakes. It is one of the core validation sites for remote sensing of soil moisture based on SMAP data. The climate in the region varies from arid to temperate with an average annual precipitation ranging from < 250 mm in the North part of the watershed to > 1150 mm at the highest elevation in the Southwest. Annual snow varies from approximately 20% of the annual precipitation in the lower elevations to > 70% at the higher elevations. The average annual temperature ranges from 7.2 °C in low elevations to 3.9 °C in high elevations. The land use is dominated by rangeland that is covered with mixed sagebrush shrubs and grasses. The topography is fairly steep. The Western part of the watershed is sparsely vegetated with very rocky soils, while the Eastern part exhibits silty soils with dense vegetation cover.

3.1.4. Big Cypress Creek, Georgia

The Big Cypress Creek Watershed (BCCW) is located in the Southwest of Georgia (GA). It covers the northern part of the Lower Flint River and the Lower Big Slough watersheds and the western part of the Horseshoe Bend-flint River watershed. The BCCW encompasses the ‘Jones Ecological Research Center’ (JERC) CRN site. The climate in the region is humid subtropical. The average annual precipitation ranges from 1140 mm in the eastern part to 1400 mm in the southern part of the watershed. The average annual temperature ranges from 15.5 °C in the North to 21 °C in the South (U.S. Geological Survey, 1986). The region is entirely flat with mixed land covers including evergreen forests with grass understory and agricultural lands. The predominant soil type is very well drained deep sand with a deep water table.

3.2. Reference soil moisture data

As mentioned earlier, CRN observations were used as the reference soil moisture data. The CRN method (Zreda et al., 2008) provides a unique opportunity to non-invasively measure effective soil moisture within the topsoil and to fill the scale gap between point-scale in situ data and large-scale remote sensing observations. Given a footprint area close to that of MODIS (detailed below), the CRN data provide an excellent means for evaluation of OPTRAM soil moisture estimates from MODIS observations.

Based on neutron transport simulations, Zreda et al. (2008) found that 86% of the neutron signal occurs within a 335-m radius at sea level, which is nearly independent of the soil moisture level. They also found that the vertical extent of the neutron signal depends on soil moisture content and ranges from about 15 cm in saturated soils to about 70 cm in very dry soils. Recent particle transport simulations show a similar footprint area in the order several hundred meters albeit with more spatial sensitivity of soil moisture within the footprint (Desilets and Zreda, 2013; Kohli et al., 2015). The exact CRN footprint and sensitivity are still an active area of research. The CRN data have been recently used for validation of spaceborne surface soil moisture products such as SMAP, SMOS, and ASCAT for COSMOS sites in the United States, Australia, Europe and Africa (Montzka et al., 2017; Akbar and Moghaddam, 2015; Fascetti et al., 2016; Van der Schalie et al., 2016). Currently, there are approximately 194 permanent CRN stations worldwide (Andreasen et al., 2017), including 73 COSMOS stations in the U.S. (Zreda et al., 2012), 20 TERENO stations in Germany (Baatz et al., 2015), 13 CosmOz stations in Australia (Hawdon et al., 2014), and 32 COSMOS-UK stations in the United Kingdom (Evans et al., 2016) all of which provide excellent data for remotely sensed soil moisture validation and evaluation experiments.

The CRN detects the ambient low-energy neutron density in the air. The low-energy neutrons are highly sensitive to the mass of hydrogen

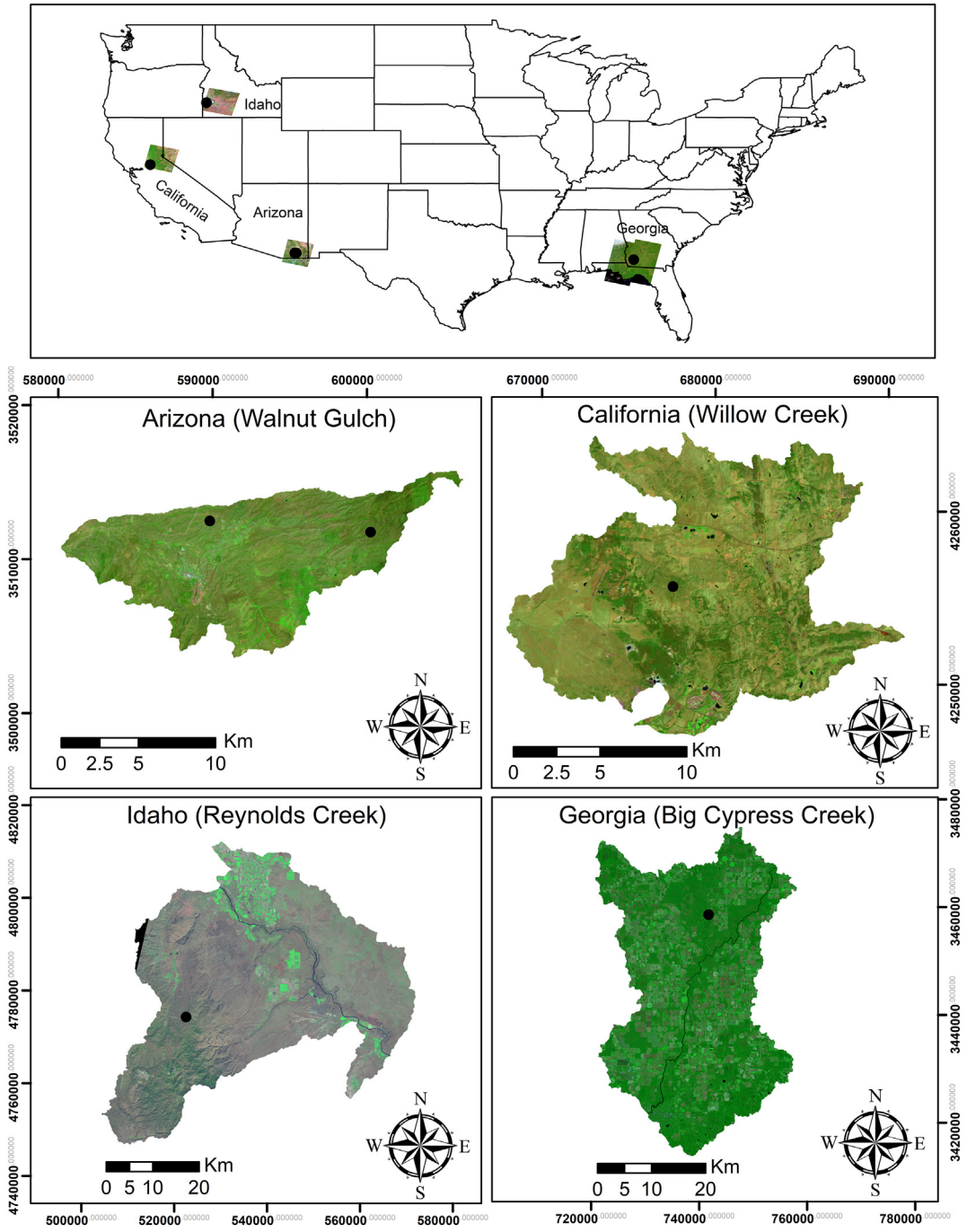

Fig. 2. Geographical locations of the watersheds considered for evaluation of OPTRAM. Landsat 8 shortwave infrared, near infrared, and green bands (September 2018) were used to create false color composite images (from bands 7–5–3) in which land surfaces covered with vegetation appear deep green. The locations of the cosmic-ray neutron soil moisture sites are marked with filled black circles. (For interpretation of the references to color in this figure legend, the reader is referred to the web version of this article.)

Table 1
Characteristics of the CRN sites within the four selected watersheds.

Watershed's name	CRN site	Temporal coverage	Latitude	Longitude	Lattice water (%)	Soil organic carbon (%)
Walnut Gulch (WGW)	Lucky Hills	13-Mar-2012 to 31-Jan-2016	31.744	−110.052	1.50	3.65
	Kendal	02-Jun-2010 to 7-Jan-2017	31.737	−109.942	2.40	0.80
Willow Creek (WCW)	Tonzi Ranch	10-May-2011 to 31-May-2017	38.432	−120.966	6.05	0.55
Reynolds Creek (RCW)	Reynolds Creek	10-Aug-2011 to 31-May-2017	43.121	−116.723	5.70	2.62
Big Cypress Creek (BCCW)	JERC	19-Sep-2011 to 16-May-2017	31.236	−84.462	1.08	0.66

and thus soil water near the ground surface (Zreda et al., 2012; Avery et al., 2016). A calibration function that relates the change in low-energy neutrons to the change in hydrogen content is commonly developed for estimation of soil moisture. The CRN is also affected by other hydrogen sources (e.g., atmospheric water vapor, soil organic matter, and mineral lattice water), and thus may provide soil moisture values exceeding the soil's porosity, especially in very humid regions (Franz et al., 2012; Bogena et al., 2013; Baatz et al., 2015). In such cases, the influence of additional sources of hydrogen should be accounted for in the CRN soil moisture calibration. For this study, we corrected the CRN soil moisture data based on the method proposed in Franz et al. (2013) and Bogena et al. (2013) as follows:

$$\theta_v = \rho_b \left[\frac{0.0808}{\left(\frac{N_{pih}}{N_0}\right) - 0.372} - 0.115 - \theta_{lw} - \theta_{soceq} \right] \quad (6)$$

where θ_v is the volumetric moisture content ($cm^3\,cm^{-3}$), θ_{lw} is lattice water content ($g\,g^{-1}$), θ_{soceq} is soil organic carbon water content equivalent ($g\,g^{-1}$), N_{pih} is the corrected neutron intensity (moderated neutron counts per time interval, cph), N_0 is a specific calibrated parameter that represents the count rate over dry soils (cph), and ρ_b is the dry soil bulk density ($g\,cm^{-3}$). The θ_{lw} and θ_{soceq} data were obtained from calibration datasets provided on the COSMOS data portal (http://cosmos.hwr.arizona.edu). More details about CRN calibration and accounting for various hydrogen sources are provided in Franz et al. (2012), Rosolem et al. (2013), Bogena et al. (2013), and Lv et al. (2014).

The precipitation data were extracted from the closest SNOwpack TELemetry (SNOTEL) and Soil Climate Analysis Network (SCAN) sites.

3.3. Satellite data

3.3.1. MODIS

The Moderate Resolution Imaging Spectroradiometer (MODIS) is a key instrument on board of NASA's Terra (EOS AM-1) and Aqua (EOS PM-1) satellites that plays an important role in studying land surface properties and processes and for the development of models to predict global change. Terra and Aqua MODIS satellites capture the entire Earth surface every 1 to 2 days and acquire data in 36 individual spectral bands (400–14,400 nm) at resolutions of 250 m (bands 1–2), 500 m (bands 3–7), and 1000 m (bands 8–36). In this study, long-term cloud-free MODIS land surface reflectance images (Terra MOD09A1 version 6) from 2001 to 2017 were acquired and analyzed. This product provides spectral reflectance at bands 1–7 with 500 m spatial resolution and 8-day temporal resolution as a gridded level-3 product in the Sinusoidal projection. Each MOD09A1 pixel contains the best possible observation during an 8-day period as selected on the basis of high observation coverage, low view angle, the absence of clouds and cloud shadows, and aerosols. Reflectance values from bands 1 (*Red*) and 2 (Near Infrared, *NIR*) were used to calculate $NDVI = (NIR - Red)/(NIR + Red)$ and reflectance from band 7 (i.e., SWIR, 2130 nm) was used for calculating *STR* with Eq. (2). The main reason for selecting band 7 reflectance is its stronger linear correlation with soil moisture content when compared with other SWIR wavelengths (e.g., 1240 and 1640 nm corresponding to MODIS bands 5 and 6), as discussed in Sadeghi et al. (2015). Because MODIS SWIR band 7 used in Eq. (2) is sufficiently far from the water vapor absorption bands in the SWIR region (i.e., 1400 and 1900 nm), the effects of atmospheric water vapor can be neglected. The images were analyzed and projected into WGS84 geographic coordinates using the HDF-EOS 2.14 tool (http://hdfeos.org/) and MATLAB R2015b (Math Works Inc., Natick, MA) software.

3.3.2. SMAP

The L-band Soil Moisture Active and Passive (SMAP) satellite has been designed and launched by NASA with the major aim of measuring and monitoring soil moisture changes (Entekhabi et al., 2010). The SMAP released 7 advanced soil moisture products as levels 2, 3, and 4 that provide surface and root zone soil moisture with spatial resolutions of 3, 9, and 36 km and temporal resolutions of 3 and 24 h. In this study, the level-3 product (L3_SM_P, descending 6:00 a.m.), derived from the single channel algorithm V-Pol (SCA-V) and resampled to a global and cylindrical 36 km resolution with Equal-Area Scalable Earth Grid (EASE-Grid 2.0) global projection, was applied and compared with CRN reference data to further evaluate the MODIS-based estimates of soil moisture with OPTRAM. This level-3 product provides a daily composite of half-orbit/swath estimates of global surface soil moisture ($0.5\,cm^3\,cm^{-3}$) derived from the brightness temperature data measured by the passive microwave radiometer.

3.3.3. SMOS

Launched in 2009, the ESA Soil Moisture and Ocean Salinity (SMOS) satellite is the first Earth observation mission dedicated to map and monitor surface soil moisture (Kerr et al., 2001). To retrieve surface soil moisture ($0.5\,cm^3\,cm^{-3}$) the SMOS campaign uses the L-band microwave emissions of the biosphere (L-MEB) radiative transfer model (Wigneron et al., 2007) and a dielectric mixing model (Mironov et al., 2009). The SMOS level-2 and level-3 soil moisture products have been successfully evaluated based on ground and satellite soil moisture datasets. A recently released daily product – SMOS-INRA-CESBIO (SMOS-IC) – has been designed by the French Institut National de la Recherche Agronomique (INRA) in collaboration with the Centre d'Etudes Spatiales de la Biosphère (CESBIO) to provide global estimations of soil moisture.

The SMOS-IC algorithm is based on L-MEB, but simpler than the SMOS level-2 and level-3 soil moisture retrieval algorithms. It is more independent from uncertainties of auxiliary data, hence, provides more robust results. In contrast to the SMOS level-2 and level-3 algorithms that correct for pixel heterogeneity, pixels are assumed homogeneous in SMOS-IC (Wigneron et al., 2012; Fernandez-Moran et al., 2017). The SMOS-IC soil moisture maps are generated as global products with a 25 km (EASE-Grid 2.0) grid size. In the current study, the daily SMOS-IC soil moisture products (https://www.catds.fr/Products) from ascending orbit were used and compared with the CRN reference data to further evaluate the MODIS-based estimates of soil moisture with OPTRAM.

3.3.4. ASCAT

The Advanced Scatterometer (ASCAT) is an active C-band microwave sensor on the METOP-A/B satellite platforms, launched in 2006. The sensor was initially designed for monitoring wind speed and wind direction over the oceans, but it has been widely used for monitoring soil moisture in terms of relative saturation (Wagner et al., 2013). The relative saturation is estimated based on a simple linear change detection retrieval algorithm which is part of the Water Retrieval Package (WARP) software (Naeimi et al., 2009). A shortcoming of this algorithm is that it considers a linear relationship between the backscatter coefficient (dB) and surface soil moisture, while assuming that surface roughness and land cover are constant in time. While ASCAT provides accurate estimates of soil moisture for bare and sparsely vegetated soils, retrievals for densely vegetated regions (e.g., tropical forests) are associated with significant errors, since backscatter from soil and vegetation cannot be separated (Wagner et al., 2013). The EUMETSAT has generated several ASCAT surface and root zone soil moisture products with daily global coverage. In the current study, we used the H109 and H110 soil moisture products from 2010 to 2016, with 12.5 km spatial sampling. The relative soil saturation was converted to volumetric moisture content via multiplying with the soil porosity found in the Harmonized World Soil Database (HWSD, Nachtergaele et al., 2012). Soil moisture data with noise designation above 20% were excluded from our analyses, while all remaining data were compared with the CRN reference data (Montzka et al., 2017).

Table 2
The dry and wet edge parameters [Eq. (5)] obtained for each watershed based on long-term MODIS satellite data.

Watershed, state	# MODIS images	Dry edge		Wet edge	
		i_d	s_d	i_w	s_w
Walnut Gulch (WGW), AZ	543	0.10	2.60	2.50	1.70
Willow Creek (WCW), CA	750	0.00	2.80	1.50	10.0
Reynolds Creek (RCW), ID	450	0.23	1.10	3.00	5.50
Big Cypress Creek (BCCW), GA	560	0.00	0.70	0.00	19.0

3.4. Data analyses

3.4.1. OPTRAM parameterization

The dry and wet edges of OPTRAM (i.e., parameters of Eq. (5)) were determined based on the pixel distribution within the *STR-NDVI* space. The dry (i_d and s_d) and wet (i_w and s_w) edge parameters were determined via fitting of a straight line to the *STR-NDVI* point clouds (see Table 2). Because of the feasibility of universal parameterization of the OPTRAM model (Sadeghi et al., 2017), an integrated *STR-NDVI* trapezoid including several hundred images acquired in the period from 2001 to 2017, was applied for each watershed. This approach aided in further reduction of time-dependency of the dry and wet edge parameters and provided "effective" model parameters for each watershed. The saturation degree (W) was mapped with Eq. (5) for each date and watershed. The estimated W values for pixels containing the CRN sites were converted to volumetric moisture contents by multiplying with the soil porosity values from the HWSD.

In our analyses, pixels with negative NDVI values were filtered to omit pixels without vegetation or soil (e.g., water surfaces, snow, rock). While Sadeghi et al. (2017) resampled Landsat-8 and Sentinel-2 images to 120-m pixel size to remove effects of oversaturated pixels, here we employed the original MODIS pixels, because oversaturated pixels are unlikely at 500-m spatial resolution, unless they cover surface water bodies. The resultant optical trapezoids for the four investigated watersheds (shown later in Fig. 3) verified this assumption, as the wet edge data were obtained within the expected *STR* range for saturated/wet land.

As suggested by Sadeghi et al. (2017), fitting the edges of the optical trapezoids was done based on visual inspection, rather than least-square regression, mainly to exclude the scattered points around the main body of the trapezoids. The visual fitting, however, introduces user bias and leads to some degree of uncertainty of model outputs. To investigate the effects of visual fitting on soil moisture results, we performed a sensitivity analysis, varying the initially visually-fitted parameters by adding randomly-generated errors in the range of ± 5%, ± 10%, ± 15%, and ± 20% of the initial values, where 4 replicates (R1 to R4 in Fig. 4) were considered for each level. To quantify the uncertainties due to visual fitting, soil moisture values calculated with perturbed parameters were compared to those obtained with the initial parameters (see Section 3.2).

3.4.2. Rescaling of soil moisture data

Soil moisture data from different sources (e.g., satellite vs. in situ, or varied satellites) typically exhibit consistent temporal evolution, but different mean and standard deviation values. Hence, rescaling data through matching the cumulative probability (CP) or cumulative distribution function (CDF) has been recommended for reducing systematic biases between different soil moisture datasets (Reichle and Koster, 2004; Koster et al., 2009; Brocca et al., 2011; Mishra et al., 2017). The CDF matching removes impacts of time-invariant errors from comparison between estimated and measured soil moisture and provides an objective basis for intercomparisons of anomalies. In this paper, we followed the strategy of Reichle and Koster (2004) and matched the CDF of remotely sensed soil moisture data to the CRN reference data (Crow et al., 2005; Kumar et al., 2012). Accordingly, we calculated the bias-corrected (rescaled) remotely sensed soil moisture, θ_{RS}, from original remotely sensed soil moisture, θ'_{RS}, as follows:

$$\theta_{RS} = \mu_{CRN} + (\theta'_{RS} - \mu_{RS})\frac{\sigma_{CRN}}{\sigma_{RS}} \tag{7}$$

where μ and σ represent the mean and standard deviation of soil moisture data, respectively, for a given location for the study period, and subscripts *RS* and *CRN* denote the corresponding data sources.

3.4.3. Performance metrics

For each comparison of pairs of remotely sensed and reference (CRN) soil moisture observations, the correlation coefficient (R), the root mean squared error (*RMSE*), bias, and unbiased *RMSE* (*ubRMSE*) were applied as follows:

$$R = \frac{Cov(\theta_{RS}, \theta_{CRN})}{\sigma_{RS}\sigma_{CRN}} \tag{8}$$

$$RMSE = \sqrt{\frac{1}{N}\sum_{i=1}^{N}(\theta_{RS} - \theta_{CRN})_i^2} \tag{9}$$

$$bias = \frac{1}{N}\sum_{i=1}^{N}(\theta_{RS} - \theta_{CRN})_i \tag{10}$$

$$ubRMSE = \sqrt{RMSE^2 - bias^2} \tag{11}$$

where i denotes a given pair of estimates and measurements and N is the total number of paired estimates and measurements. Because the CRN stations are not exactly aligned with the centers of satellite RS pixels (MODIS, SMAP, SMOS, and ASCAT), all pixels covering at least 50% of the CRN footprint were used for calculating these metrics.

3.4.4. Drought analysis

Most of the proposed drought assessment indices are based on long-term atmospheric variables (Palmer, 1965; McKee et al., 1993; Hogg and Hurdle, 1995), but they do not consider soil moisture measurements, which are a direct measure of agricultural drought. One reason for this negligence is probably due to a lack of soil moisture monitoring networks in the past. Today, satellite data can provide soil moisture information with a wide range of spatial and temporal resolutions. MODIS satellite data provide an excellent long-term database for drought monitoring applications. With respect to its definition, agricultural drought is defined based on the soil moisture deficit and its effect on crop production, i.e., when evapotranspirative losses exceed the plant available soil moisture defined as the difference between soil moisture at field capacity and that at permanent wilting point (Kabat and Beekma, 1994). Martinez-Fernandez et al. (2015) introduced a Soil Water Deficit Index (SWDI) for agricultural drought monitoring as follows:

$$SWDI = 10\frac{\theta - \theta_{FC}}{\theta_{FC} - \theta_{PWP}} \tag{12}$$

where θ_{FC} and θ_{PWP} ($cm^3\,cm^{-3}$) are soil moisture content at field capacity and permanent wilting point, respectively. Positive values of SWDI signify excess water in the soil, while negative values indicate some degree of soil drought. When SWDI is equal to zero, the soil is at field capacity moisture content. The values equal to or smaller than −10 indicate that the moisture content is below the lower limit of available water for plants, i.e., extreme water deficit in soil (Martinez-Fernandez et al., 2015). As mentioned above, MODIS-OPTRAM soil moisture estimates can provide a long-term dataset for agricultural drought monitoring based on calculating SWDI (i.e., OPTRAM-SWDI). The θ_{FC} and θ_{PWP} were determined with the ROSETTA pedotransfer model (Schaap et al., 2001) that uses clay content, sand content, silt content, and bulk density data for parameterizing a soil water retention model (i.e., van Genuchten, 1980) and thereby determining θ_{FC} and θ_{PWP}. These basic soil properties were extracted for each site from the

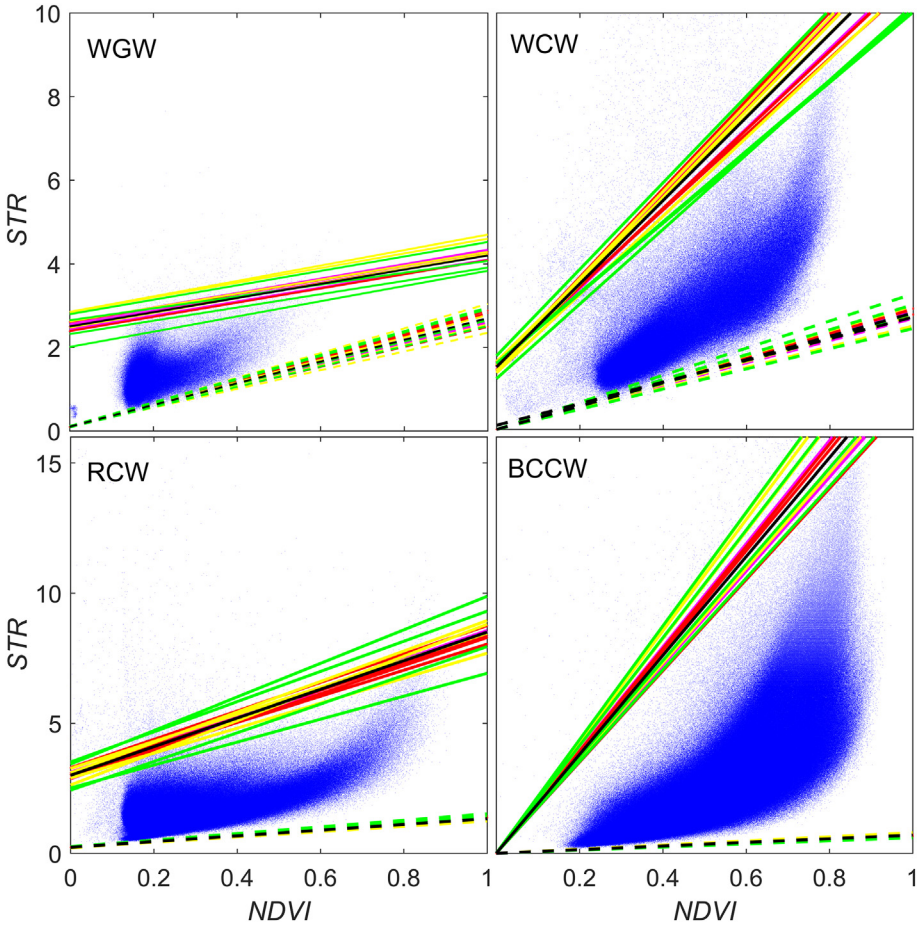

Fig. 3. Pixel distribution within the *STR-NDVI* space formed with long-term MODIS data (2001–2017) for the Walnut Gulch Watershed (WGW), Willow Creek Watershed (WCW), Reynolds Creek Watershed (RCW), and Big Cypress Creek Watershed (BCCW). The solid and dashed black lines represent the best visually fitted wet and dry edges, respectively. The colored lines, used for sensitivity analysis, show randomly varied edges at levels of ± 5% (magenta with 4 replicates), ± 10% (red with 4 replicates), ± 15% (yellow with 4 replicates), and ± 20% (green with 4 replicates). (For interpretation of the references to color in this figure legend, the reader is referred to the web version of this article.)

global ISRIC Soil database (https://soilgrids.org) with a spatial resolution of 250 m.

The Crop Moisture Index (CMI) (Palmer, 1968) which is related to soil water storage was used as reference to assess the accuracy of the OPTRAM-SWDI for agricultural drought monitoring. The daily CMI is inversely calculated based on the subtraction of daily potential evapotranspiration from daily precipitation ($P - ET_0$), where the daily ET_0 was calculated based on the Thornthwaite method for each site (Thornthwaite, 1948; Rim, 2000).

4. Results and discussion

4.1. OPTRAM parameters

Fig. 3 illustrates the pixel distribution within the *STR-NDVI* space for each watershed. The black lines represent the optimized dry and wet edges and the colored lines represent the randomly perturbed edges used for sensitivity analysis. As observed, a nearly trapezoidal shape is formed by *STR-NDVI* point clouds for each watershed based on the integration of all MODIS images listed in Table 2. Each of the four feature spaces exhibit a wide range of *STR* and *NDVI* values that may be due to the variability of soil moisture, diverse climate, soil type, and land cover. In general, *STR* and *NDVI* values are larger for regions with dense vegetation cover, e.g., Willow Creek and Big Cypress Creek watersheds (see also Fig. 2), which is due to high soil moisture and/or vegetation water content. The larger *STR* values in densely vegetated soils indicate higher moisture contents in the root zone. The visually optimized parameters for the dry and wet edges for each watershed are listed in Table 2. Using these parameters, *W* in Eq. (5) can be computed for any value of *STR* and *NDVI*.

4.2. Sensitivity of OPTRAM outputs to model parameters

Sensitivity of OPTRAM-based soil moisture estimates at CRN pixels to the model parameters is shown in Fig. 4, where correlations between soil moistures estimates using the best visually fitted parameters and the randomly perturbed parameters are shown. In general, strong correlations are observed for all the uncertainty levels. The average RMSE values at levels ± 5%, ± 10%, ± 15%, and ± 20% for all the sites are 0.007, 0.010, 0.012, and 0.025 $cm^3\,cm^{-3}$, respectively, indicating that the OPTRAM outputs are not very sensitive to the model parameters. Based on Fig. 4, uncertainties due to the visual fitting approach are anticipated to be significantly less than the errors of optical or microwave remote sensing approaches (presented later). In other words, the visual fitting approach results in acceptable soil moisture estimates, despite its perceived user bias.

4.3. Rescaled CDFs

Comparisons between the original and rescaled CDFs of CRN reference soil moisture data and soil moisture estimates from OPTRAM, SMAP, SMOS, and ASCAT for each site and for all dates are illustrated in Fig. 5. A large mismatch is shown between the original CDFs, while the rescaled CDFs coalesced well. This result indicates that the different sources resulted in different, but highly-correlated, soil moisture values. One probable reason for the observed mismatch could be the spatial scale mismatch, i.e., different image pixel size and sensing volume. As seen in Fig. 5, ASCAT tends to produce lower soil moisture values for most sites. For example, at the Kendal and Lucky Hills sites, the ASCAT soil moisture estimates indicate very dry conditions ($< 0.05\,cm^3\,cm^{-3}$) during most of the dry season, while OPTRAM never reached values that low. The highest soil moisture values in most sites were reported by

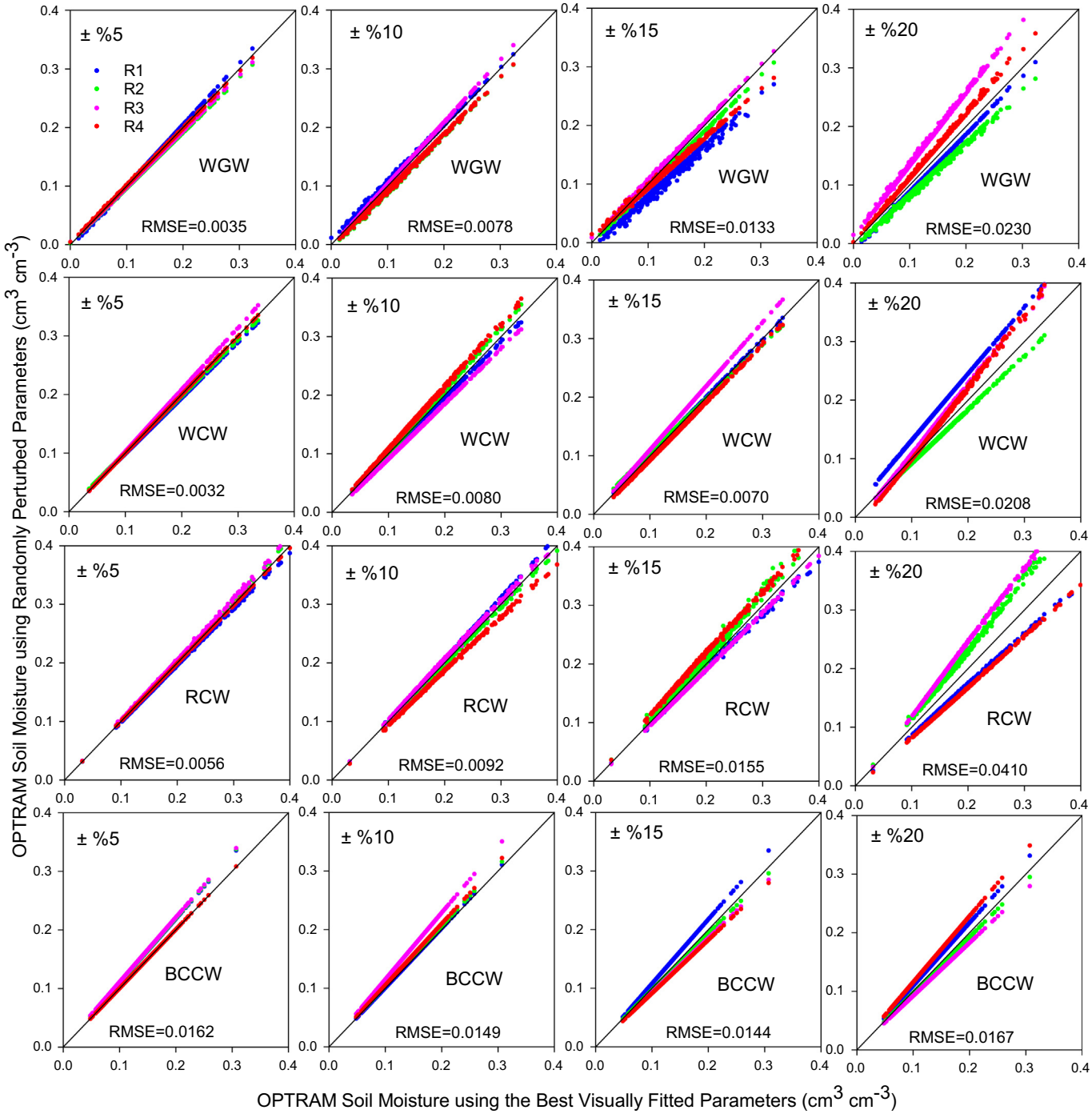

Fig. 4. OPTRAM soil moisture estimates at CRN sites using the best visually fitted parameters (Table 2) against randomly perturbed parameters used for sensitivity analysis for ranges of ± 5%, ± 10%, ± 15%, and ± 20%. Each row of plots shows data from a different site: Kendal, AZ (WGW), Tonzi Ranch, CA (WCW), Reynolds Creek, ID (RCW), and JERC, GA (BCCW). The root mean squared error (RMSE) denotes averaged values of the RMSE from 4 replicate data sets (i.e., R1-R4) shown in different colors.

either OPTRAM or SMAP, which could be due to their deeper sensing depth, i.e., deeper penetration of SMAP's L-band and OPTRAM's responsiveness to plant canopy-derived root zone soil moisture. As mentioned, the rescaled CDFs for the remotely sensed soil moisture data were well matched to CRN soil moisture data at all four sites, leading to reduced error metrics such as *RMSE* and *bias*. However, it should be noted that the correlation coefficient (R) will not change due to CDF matching, as CDF matching is basically a linear transformation of the original data and has nothing to do with random variations that determine R.

4.4. Soil moisture estimates

Fig. 6 depicts a comparison of OPTRAM-derived soil moisture daily temporal dynamics with those of CRN, SMAP, SMOS and ASCAT from 2010 to 2017. The OPTRAM estimates exhibit distinct dry and wet cycles and capture the dynamics of CRN soil moisture at the five selected sites, especially at Tonzi Ranch and Reynolds Creek, indicating good performance of OPTRAM (mean *ubRMSE* value of 0.0675 and mean R value of 0.3940). Data shown in Fig. 6 clearly demonstrate distinct differences in climate, land cover and soil variability among the

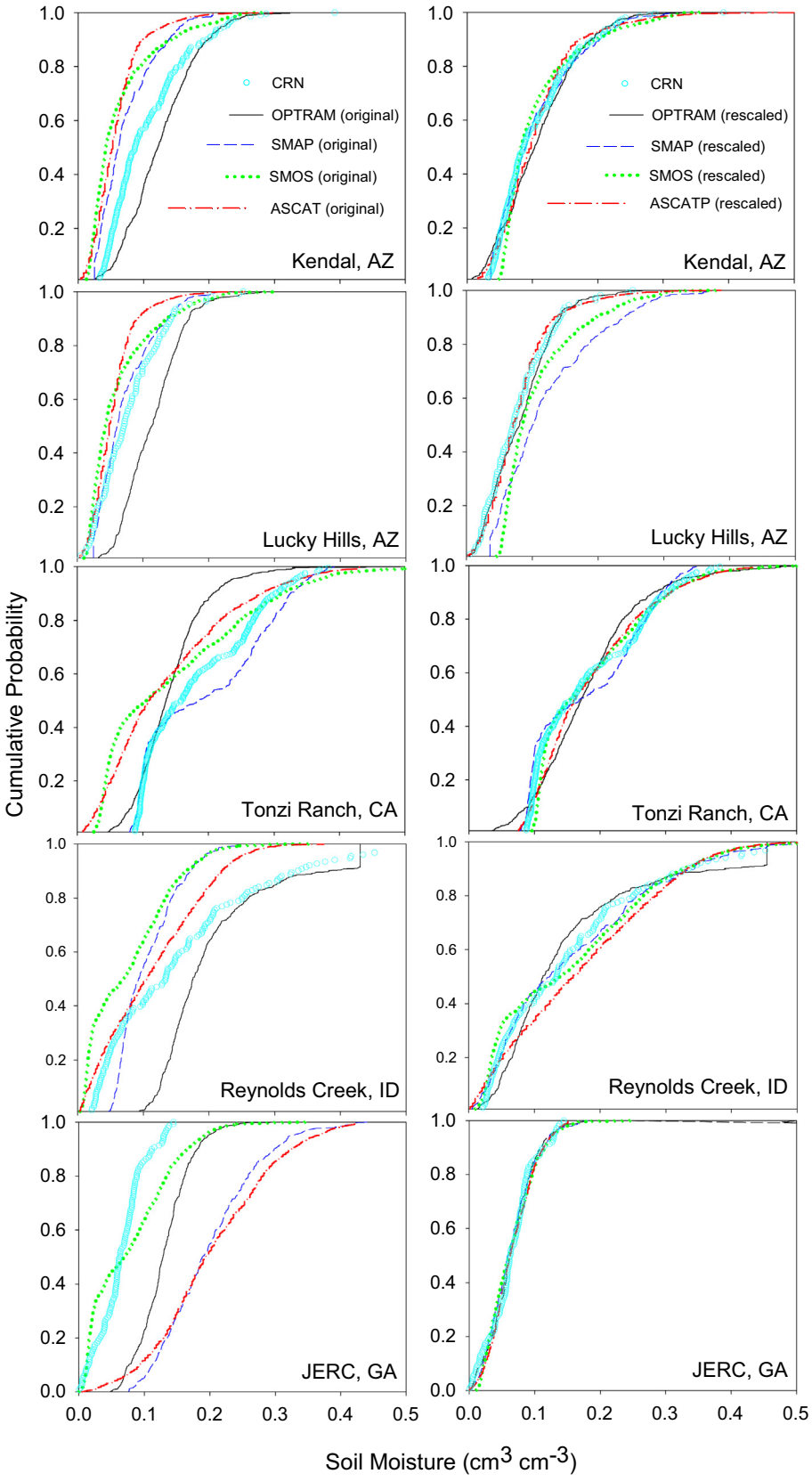

Fig. 5. Cumulative probability for matching the CDFs based on CRN data, original (left column) and rescaled (right column) remote sensing-based estimates of soil moisture from OPTRAM, SMAP, SMOS, and ASCAT for sites Kendal, AZ; Lucky Hills, AZ; Tonzi Ranch, CA; Reynolds Creek, ID; and JERC, GA.

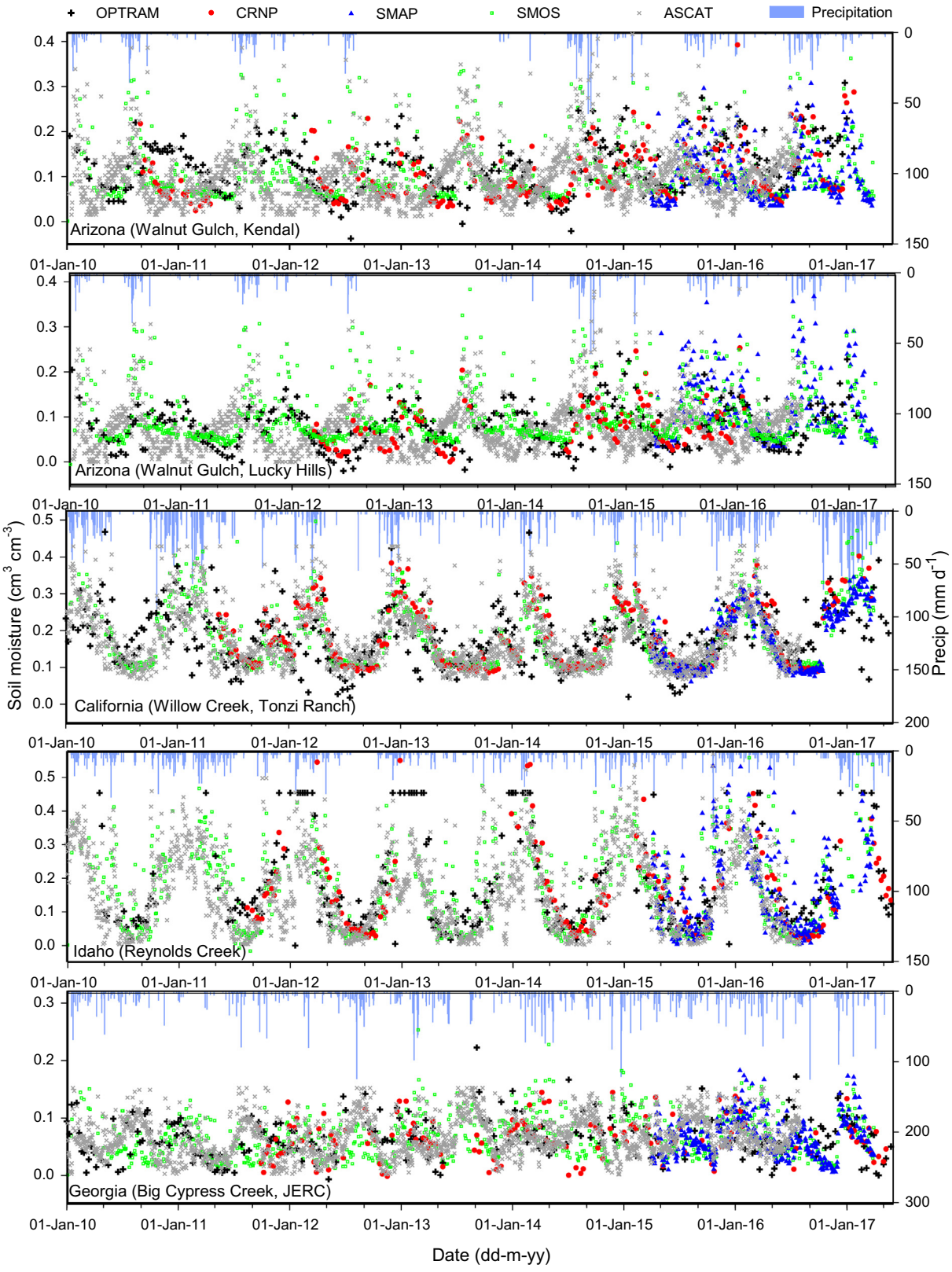

Fig. 6. Time series of remotely sensed (OPTRAM, SMAP, SMOS, ASCAT) and CRN-based soil moisture and precipitation at Kendal, AZ; Lucky Hills, AZ; Tonzi Ranch, CA; Reynolds Creek, ID, and JERC, GA. The precipitation data were extracted from SNOTEL (SNOwpack TELemetry) and SCAN (Soil Climate Analysis Network) sites closest to each CRN station. Note that for the Walnut Gulch sites, no precipitation was recorded by the SCAN rain gauges from August 2012 to November 2013.

four watersheds. Compared to the other three sites, the range of OPTRAM and CRN soil moisture is limited at Kendal and Lucky Hills (Walnut Gulch) sites because these two sites have a semi-arid climate with well-drained coarse-textured soils and limited precipitation. A wider range of soil moisture content is evident for Tonzi Ranch and Reynolds Creek, which is associated with more frequent precipitation events during each season and also the existence of clay loam and silty soils across these two sites. In addition, a wider range of OPTRAM soil moisture compared to CRN observations is also evident at each site during the studied period, especially for humid climates. This is partly due to the higher noise of the satellite-based estimates compared with the noise of ground (CRN) measurements. Another physical reason, especially for bare soils, is that OPTRAM-based estimates represent the surface (skin) soil moisture for a thin layer with a few mm depth, whereas CRN data provide effective soil moisture down to about 50 cm for nearly dry soils (Zreda et al., 2012). This fact results in remotely sensed soil moisture values to be more responsive to atmospheric factors (i.e., precipitation, radiation, and evaporative demand), explaining the high temporal variability and dynamic range of surface soil moisture. The CRN soil moisture values are generally higher during summer and dry periods. This result is mainly due to the neglected effect of high biomass growth rate affecting CRN-based soil moisture (Andreasen et al., 2017).

In Fig. 6, rescaled OPTRAM soil moisture estimates are also compared with rescaled soil moisture retrievals from SMAP, SMOS, and ASCAT. As seen, OPTRAM estimates follow the seasonal variations of SMAP, SMOS, and ASCAT retrievals. Although a similar overall pattern is observed, the OPTRAM values are generally lower, especially during warmer periods. During or shortly after a precipitation event, OPTRAM data are quite noisy, which may be due to low quality MODIS optical images resulting from cloud and atmospheric water vapor effects.

The original ASCAT, SMOS, and SMAP soil moisture retrievals (not presented here) were much more variable showing a wider range of values than those of OPTRAM and CRN for most sites. This greater variability may primarily be due to the different sensing depths of microwaves, which are known to be shallower for shorter wavelengths. For instance, C-band ASCAT is sensitive down to a 2 cm depth and can be even < 1 cm during a strong rainfall event, whereas L-band SMOS penetrates to about 5 cm (Al-Yaari et al., 2014). Therefore, during and shortly after a precipitation event, microwave soil moisture retrievals associated with a very wet surface layer show higher soil moisture values than CRN data with the penetration depth exceeding 15 cm. This discrepancy between microwave and CRN data is reduced with time after precipitation because the soil profile tends toward a more uniform moisture distribution. Another reason for the observed discrepancies could be due to high spatial soil moisture variability after intense precipitation events (also spatially variable), magnifying effects of the scale mismatch between lower resolution microwave and higher resolution CRN observations. For some cases, for example the Arizona sites, a time lag is observed for ASCAT soil moisture data, when moisture values fall below $0.20\,cm^3\,cm^{-3}$. This time lag can be attributed to the temporal variations of surface roughness and land cover, which are assumed to be constant in the ASCAT retrieval algorithm (WARP) (Wagner et al., 2013). The lag over summer can be related to the increase in vegetation cover and thereby decrease in soil moisture content due to plant water uptake.

Scatterplots between CRN-derived and remotely-sensed soil moisture estimates for each site are presented in Fig. 7. Correlations between the CRN estimates and rescaled OPTRAM and microwave satellite soil moisture estimates range between 0.100 and 0.927. Based on *RMSE* estimates, SMAP and SMOS performed better than OPTRAM and ASCAT in most sites. This was generally expected since microwave signals at lower frequencies (L-band) are much more sensitive to soil water (i.e., dielectric constant) and microwave-based retrievals provide more accurate soil moisture estimates than optical methods. In our study, comparison of OPTRAM estimates with ASCAT retrievals (C-band) over all sites indicate that OPTRAM performed similar to or better than ASCAT for all sites, except for the JERC site in GA.

Table 3 compares soil moisture estimation performance of OPTRAM and microwave satellites with CRN estimates in terms of *R*, *RMSE*, *unRMSE*, and *bias* for each site. These error metrics indicate a generally good agreement between the OPTRAM and CRN estimates. OPTRAM yields slightly larger *RMSE* values than SMAP and SMOS, but performs equal to or better than ASCAT for most sites. At Kendal, Lucky Hills and JERC, OPTRAM performed well with *RMSE* and *ubRMSE* close to ASCAT. OPTRAM yielded *ubRMSE* values between 0.0501 and $0.0853\,cm^3\,cm^{-3}$ and *R* values between 0.100 and 0.746 when compared with CRN. At the JERC site in GA, OPTRAM shows the best agreement with CRN, where *ubRMSE* was 0.0501 and *bias* was $0.0066\,cm^3\,cm^{-3}$. At all sites except Tonzi Ranch, OPTRAM overestimated soil moisture with an average *bias* of $0.019\,cm^3\,cm^{-3}$. This overestimation was referred to as an “oversaturated issue” in the original OPTRAM model development (Sadeghi et al., 2017), explained as the result of temporary shallow surface ponding and/or canopy interception of water, which increase the *STR* values for a given *NDVI* and thereby overestimate soil moisture content. At Tonzi Ranch, OPTRAM slightly underestimated soil moisture with a *bias* of $-0.011\,cm^3\,cm^{-3}$.

In theory, the ASCAT sensor should provide more accurate retrievals of soil moisture owing to the greater sensitivity of active microwave reflections to dielectric permittivity of soil water. The relatively large errors observed for ASCAT (compared to SMAP and SMOS) are consistent with several studies. Peng et al. (2015) found a *RMSE* value of 0.096 and a bias value of $-0.053\,cm^3\,cm^{-3}$ for ASCAT soil moisture retrievals for southwestern China. Rötzer et al. (2014) obtained *RMSE* values between 0.07 and $0.09\,cm^3\,cm^{-3}$ and a *R* value of 0.25 for ASCAT for agricultural lands within the Ruhr catchment in Germany, and Djamai et al. (2015) reported *RMSE* values ranging from 0.07 to 0.11 and *R* values from 0.10 to 0.37 for ASCAT for agricultural land and forests in Canada. In conformity with Montzka et al. (2017), the lowest error metrics are found for the SMAP and SMOS retrievals with very similar *R* values but somewhat larger *ubRMSE* values, likely due to the number of data points, study period, and use of corrected CRN data [see Eq. (6)]. Considering five site averages, the SMAP retrievals provide the highest *R* (0.77) and lowest *ubRMSE* ($0.061\,cm^3\,cm^{-3}$) values followed by SMOS retrievals ($R = 0.64$ and $ubRMSE = 0.058\,cm^3\,cm^{-3}$), and ASCAT products ($R = 0.40$ and $ubRMSE = 0.076\,cm^3\,cm^{-3}$). At the Kendal, Lucky Hills and JERC sites, SMAP soil moisture retrievals fall within the mission target accuracy of $0.04\,cm^3\,cm^{-3}$.

Considering data bias, SMAP tends to slightly underestimate soil moisture at Kendal, Reynolds Creek, and JERC and the ASCAT underestimates soil moisture at Tonzi Ranch and Reynolds Creek. Underestimations for SMAP may arise from the smaller sensing depth and larger radiometer footprint compared with CRN measurements, as discussed above. For ASCAT the underestimation could additionally be due to the uncertainty in soil porosity when the relative saturation (values between 0 and 1) is converted to volumetric moisture content. The underestimation could also be due to bias in CRN measurements. For instance, the Tonzi Ranch site is located in a flat area where the CRN footprint is subject to water ponding after heavy precipitation events, resulting in higher CRN soil moisture values. At the Reynolds Creek site located in a mountainous area, the CRN footprint includes a surface layer of snow during the winter. This can result in soil moisture estimates exceeding the soil porosity, as indicated in Fig. 6.

At the JERC site, remotely sensed data exhibit the smallest bias scores, which may arise from the narrow range of soil moisture dynamics. For instance, OPTRAM shows *R* equal to 0.10 but *ubRMSE* equal to $0.0501\,cm^3\,cm^{-3}$. This result indicates that the use of these standard metrics is not always suitable for in-depth evaluation of soil moisture accuracy. The correlation between in situ soil moisture and satellite observations is commonly not very large and a typical *R* range between 0.40 and 0.80 is reported, but even a complete lack of correlation does not necessarily mean that the satellite based estimations are

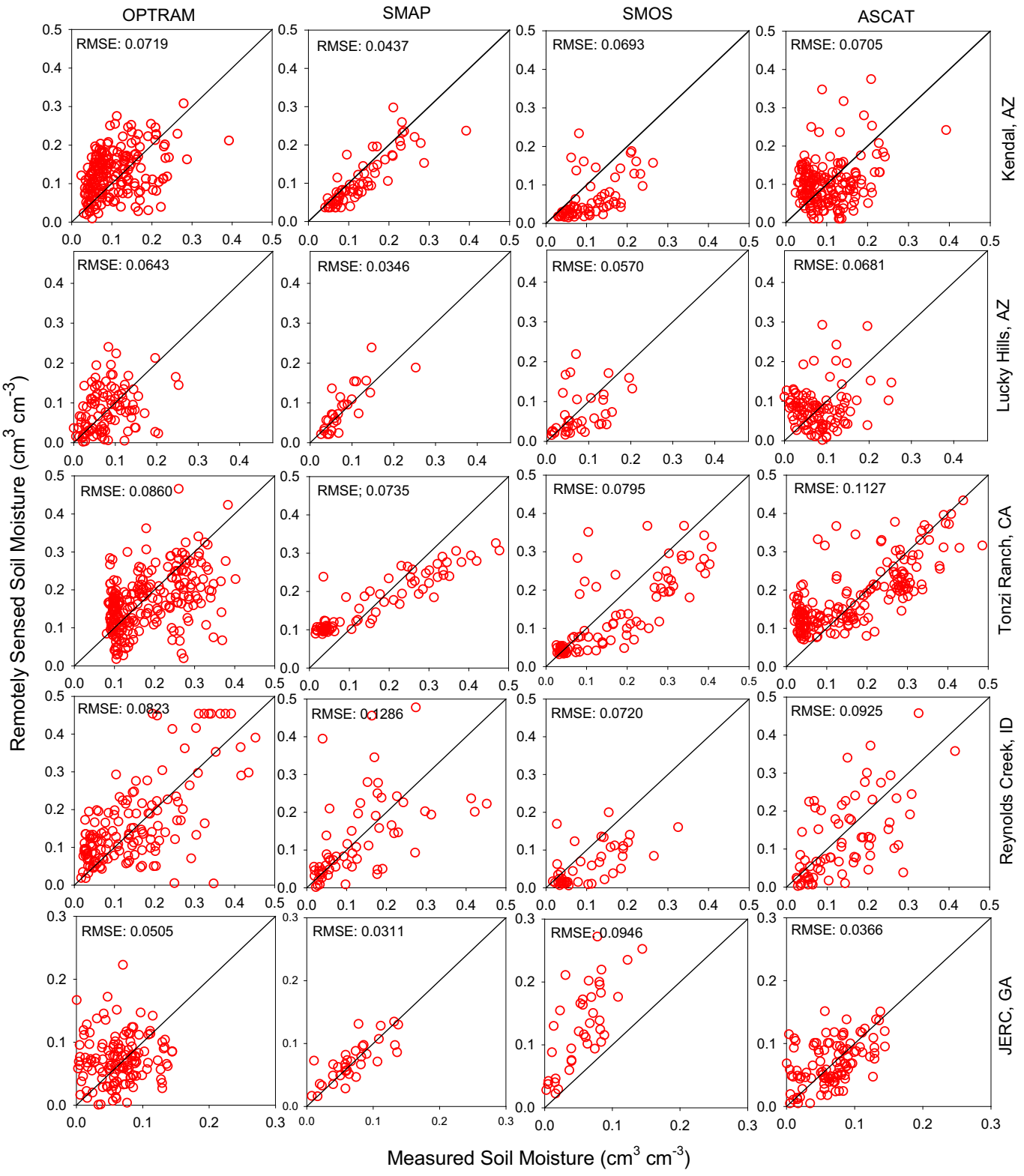

Fig. 7. Scatterplots comparing remotely sensed (OPTRAM, SMAP, SMOS, and ASCAT) with CRN-based soil moisture for Kendal, AZ; Lucky Hills, AZ; Tonzi Ranch, CA; Reynolds Creek, ID, and JERC, GA.

wrong (Wagner et al., 2013). In such a case, as we have done in this study, it is more appropriate to interpret remote sensing results in a relative context for example by comparing with performance of other satellite data against the same reference data rather than attributing absolute meaning to the results (Wagner et al., 2013).

4.5. Drought indices

As mentioned earlier, long-term MODIS data can provide a historical database of soil moisture estimates preceding the launch of microwave satellites. This long-term database is a valuable asset for an array of applications such as agricultural drought assessment and

Table 3
Performance metrics for evaluation of OPTRAM, SMAP, SMOS, and ASCAT soil moisture estimates based on CRN observations at each of the investigated sites.

CRN site	Metric	OPTRAM	SMAP	SMOS	ASCAT
Kendal, AZ	*bias*	0.0186	−0.0216	0.0452	0.0015
	ubRMSE	0.0695	0.0380	0.0525	0.0705
	RMSE	0.0719	0.0437	0.0693	0.0705
	R	0.3533	0.8522	0.5629	0.2629
	N	201	63	67	172
Lucky Hills, AZ	*bias*	0.0399	0.0069	0.0102	0.0015
	ubRMSE	0.0504	0.0339	0.0561	0.0680
	RMSE	0.0643	0.0346	0.0571	0.0681
	R	0.3098	0.7892	0.4243	0.1609
	N	108	28	37	101
Tonzi Ranch, CA	*bias*	−0.0109	0.0065	0.0327	−0.0076
	ubRMSE	0.0853	0.0732	0.0725	0.1125
	RMSE	0.0860	0.0735	0.0795	0.1127
	R	0.461	0.927	0.7918	0.752
	N	244	74	90	206
Reynolds Creek, ID	*bias*	0.0109	−0.0070	0.0424	−0.0094
	ubRMSE	0.0822	0.1284	0.0582	0.0921
	RMSE	0.0823	0.1286	0.0720	0.0925
	R	0.7460	0.5041	0.6202	0.6104
	N	177	64	43	73
JERC, GA	*bias*	0.0066	−0.0015	−0.0792	0.0015
	ubRMSE	0.0501	0.0310	0.0517	0.0365
	RMSE	0.0505	0.0311	0.0946	0.0366
	R	0.1000	0.7829	0.7907	0.4977
	N	139	36	41	109

N: the number of data pairs used to calculate metrics.

climate studies. To check the performance of OPTRAM for this application, SWDI was computed based on OPTRAM estimates and compared with an atmospheric drought index, CMI. Weekly SWDI temporal dynamics based on OPTRAM soil moisture estimates for our five selected sites are compared with CMI values in Fig. 8 (left). In this study, the OPTRAM-SWDI approach is similar to Mishra et al. (2017) and Martinez-Fernandez et al. (2016), who used SMAP and SMOS soil moisture retrievals to compute SWDI to monitor agricultural drought, respectively. A similar pattern is observed between OPTRAM-SWDI and CMI at all sites except the Big Cypress Creek, which shows large discrepancies over the whole period in terms of temporal evolution and identification of drought onsets. This mismatch may arise from the narrow range of soil moisture in what is a predominantly sandy textured soil of the Big Cypress Creek (see Fig. 6). The relatively low water storage capacity (θ_{FC} and θ_{PWP} equal to 0.13 and 0.05 respectively) limits plant soil moisture availability, producing larger differences in calculated soil moisture based on CMI (i.e., $P - ET_0$). The OPTRAM-SWDI is an indicator of water availability in soil, which can be used to estimate agricultural drought.

Fig. 8 (right) provides a comparison between OPTRAM soil moisture and *NDVI* time series for each site for the 2001 to 2017 period. It is obvious that OPTRAM soil moisture and *NDVI* show similar temporal evolution for the dry and wet periods (with a small time lag), which is related to the response of vegetation to soil moisture content. The OPTRAM soil moisture and *NDVI* also show similar patterns with the corresponding OPTRAM-SWDI and CMI values at each site. The *NDVI* and other similar vegetation indices such as Soil Adjusted Vegetation Index (SAVI by Huete, 1988) and Enhanced Vegetation Index (EVI by Liu and Huete, 1995) have been widely used for drought monitoring through correlation with other climatic drought indicators. However, *NDVI* anomalies may show time lags of several weeks with atmospheric variables (e.g., precipitation as discussed by Zhang et al., 2013) that restrict the application of *NDVI* for drought monitoring, as is also evident in Fig. 8 (right).

Based on OPTRAM-SWDI values, all sites have experienced a wide range of drought severity from no drought (SWDI ≥ 0) to extreme drought (SWDI ≤ −10) during the 2001 to 2017 period. In general, drought events are clearly captured by OPTRAM-SWDI based on higher negative values. For example, in Arizona a significant deficit of precipitation from May 2002 to October 2004 and February 2006 to November 2007 led to severe and extreme drought conditions evidenced by OPTRAM-SWDI values that reduced to around −17 and daily CMI values that reduced to around −5. This drought pattern coincides with the U.S. Drought Monitor data (https://droughtmonitor.unl.edu) in Arizona where > 50% of the state area experienced exceptional and extreme drought conditions during this period (data are not shown). These results are promising and indicate the importance of long-term MODIS data (since 2000) for generating historical long-term soil moisture dynamics with the OPTRAM approach to show agricultural drought periods, particularly in regions where soil moisture information is lacking. This could also potentially provide means for long-term (decadal-scale) drought monitoring based on OPTRAM-MODIS soil moisture information, which is key to developing early warning systems for agricultural drought.

A critical issue of soil moisture estimation from optical satellite data is that estimates are limited to the surface soil layer (i.e., a few mm). Agricultural drought is related to soil water availability for plants, water which is mainly stored in the deeper root zone layer. However, strong correlations exist between surface (or near-surface) and root zone soil moisture (Albergel et al., 2008; Hirschi et al., 2014). With OPTRAM, it is assumed that θ (or W) in Eq. (5) is correlated to root zone soil moisture through the vegetation response to soil water deficit in the root zone layer (Sadeghi et al., 2017). Many other studies have tracked the change in root zone soil moisture via remotely sensed vegetation indices because soil moisture status in the root zone influences the vegetation water content and thereby changes the spectral characteristics of the vegetation (Santos et al., 2014). These findings suggest that OPTRAM soil moisture estimates can be directly used for agricultural drought monitoring and that they would be a suitable alternative for microwave-based soil moisture retrievals, which are currently too coarse for drought monitoring of individual agricultural fields.

5. Summary and conclusions

This paper presents a comprehensive evaluation of the OPtical TRApezoid Model (OPTRAM) for estimation of soil moisture. The evaluation includes four distinct watersheds in the U.S., which are diverse in climate and land cover. Long-term MODIS images from 2001 to 2017 were employed to obtain a universal parameterization of the OPTRAM model for estimation of soil moisture. Cosmic-ray neutron (CRN) soil moisture data from the U.S. COSMOS network, as well as three other existing satellite-based surface soil moisture products, including SMAP, SMOS, and ASCAT retrievals, were used to evaluate OPTRAM's accuracy. The reference CRN soil moisture exhibits an area of influence similar to the size of a MODIS pixel. This similarity helps to reduce uncertainties in the comparisons. The CDF matching method was applied to eliminate bias (time-invariant errors) and to rescale OPTRAM and microwave-based soil moisture estimates. Long-term MODIS data (since 2001) was used to map long-term soil moisture dynamics with OPTRAM and to track environmental changes. For example, a soil water deficit index (OPTRAM-SWDI) was calculated based on OPTRAM soil moisture estimates and a soil water availability concept was introduced to explore the potential of OPTRAM-MODIS to monitor agricultural drought. The OPTRAM-SWDI was compared with an atmospheric drought index (CMI) to identify and capture drought dynamics for diverse climates, soil types and land covers.

Matching the CDFs significantly decreased the estimation errors (*bias*, *RMSE*, *ubRMSE*), while having no impact on *R* values. It was found that the original OPTRAM and microwave soil moisture estimates were highly correlated with CRN soil moisture at each site. OPTRAM successfully captured the temporal dynamics of the SMAP, SMOS, and ASCAT soil moisture retrievals for all sites. OPTRAM performed well for all test sites with *ubRMSE* ranging from 0.0501 to 0.0853 $cm^3\ cm^{-3}$ and

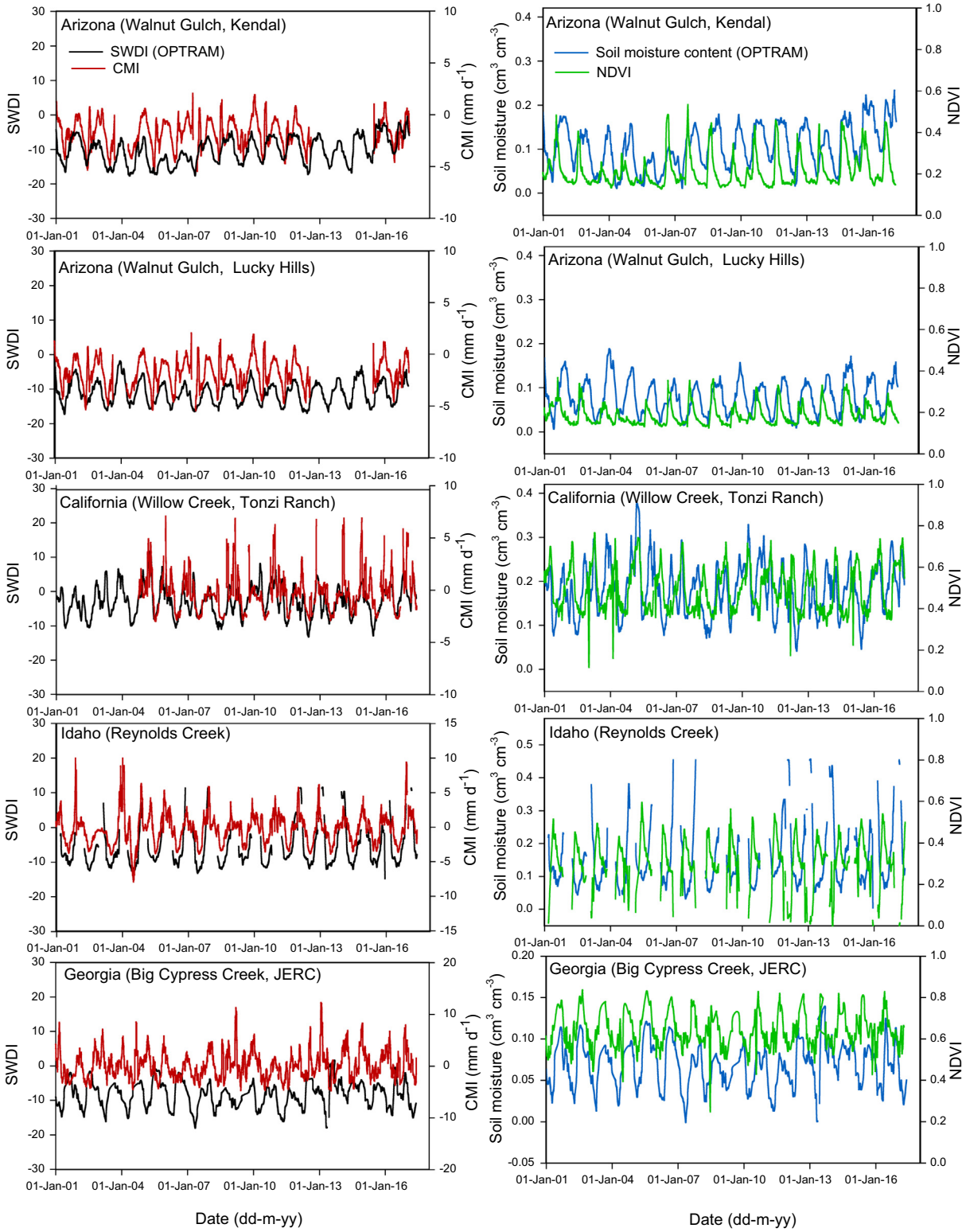

Fig. 8. Temporal dynamics of weekly OPTRAM-SWDI compared with CMI (left), and OPTRAM-based soil moisture and NDVI values (right) for five sites.

R ranging from 0.10 to 0.70. The SMAP and SMOS retrievals were more accurate than the OPTRAM estimates for most CRN sites, verifying higher sensitivity of passive microwaves to soil moisture than optical reflectance observations. The OPTRAM, however, performed similar to or slightly better than the ASCAT sensor.

A universal parameterization of OPTRAM can be obtained for a given region based on long-term MODIS data. In this study we used a visual inspection approach for delineating the dry and wet edges. A performed sensitivity analysis indicates that OPTRAM outputs are not highly sensitive to the dry and wet edge model parameters. Nonetheless, in our ongoing work we strive to develop a physical edge detection approach to eliminate any potential user bias.

Due to moderate spatial and high temporal resolution of MODIS images, OPTRAM estimates could be helpful for monitoring soil

moisture for agricultural fields and the *STR-NDVI* space could be used for downscaling of microwave satellite soil moisture products.

A similar pattern was observed between OPTRAM-SWDI and CMI at most sites. The drought events were clearly captured by OPTRAM-SWDI. These results demonstrate that the OPTRAM-SWDI is able to adequately capture drought dynamics for a wide range of climate, soil type and land cover conditions, portending OPTRAM's feasibility as a tool for agricultural drought monitoring. The calculation of SWDI is based on soil water retention parameters such as the field capacity and the permanent wilting point. The international soil datasets such as the Harmonized World Soil Database (FAO/ISRIC/ISSCAS/JRC, 2012) in conjunction with a pedotransfer function approach can provide good estimates of soil water retention parameters. Thus, where soil property databases are available, SWDI can be estimated from the OPTRAM.

Acknowledgments

The authors gratefully acknowledge funding from the National Science Foundation (NSF) grant no. 1521469 and acknowledge use of data from the COsmic-ray Soil Moisture Observing System (COSMOS), funded by the US National Science Foundation (ATM-0838491).

References

Akbar, R., Moghaddam, M., 2015. A combined active passive soil moisture estimation algorithm with adaptive regularization in support of SMAP. IEEE Trans. Geosci. Remote Sens. 53 (6), 3312–3324.

Albergel, C., Rudiger, C., Pellarin, T., Calvet, J.C., Fritz, N., Froissard, F., Martin, E., 2008. From near-surface to root-zone soil moisture using an exponential filter: an assessment of the method based on in-situ observations and model simulations. Hydrol. Earth Syst. Sci. 12, 1323–1337.

Al-Yaari, A., Wigneron, J.-P., Ducharne, A., Keer, Y.H., Wagner, W., De Lannoy, G., Reichle, R., Al Bitar, A., Dorigo, W., Richaume, P., Mialon, A., 2014. Global scale comparison of passive (SMOS) and active (ASCAT) satellite based microwave soil moisture retrievals with soil moisture simulations (MERRA-Land). Remote Sens. Environ. 152, 614–626.

Andreasen, M., Jensen, K.H., Desilets, D., Franz, T.E., Zreda, M., Bogena, H.R., Looms, M.C., 2017. Status and perspectives on the cosmic-ray neutron method for soil moisture estimation and other environmental science applications. J. Hydrol. 16 (8).

Avery, W.A., Finkenbiner, C., Franz, T.E., Wang, T., Nguy-Robertson, A.L., Suyker, A., Arkebauer, T., Arriola, F.M., 2016. Incorporation of globally available datasets into the roving cosmic-ray neutron probe method for estimating field-scale soil water content. Hydrol. Earth Syst. Sci. 20, 3859–3872.

Baatz, R., Bogena, H.R., Franssen, H.-J.H., Huisman, J.A., Montzka, C., Vereecken, H., 2015. An empirical vegetation correction for soil moisture content quantification using cosmic ray probes. Water Resour. Res. 51, 2030–2046.

Babaeian, E., Homaee, M., Montzka, C., Vereecken, H., Norouzi, A.A., van Genuchten, M.T., 2016. Soil moisture prediction of bare soil profiles using diffuse spectral reflectance information and vadose zone flow modeling. Remote Sens. Environ. 187, 218–229.

Bartalis, Z., Wagner, W., Naeimi, V., Hasenauer, S., Scipal, K., Bonekamp, H., Figa, J., Anderson, C., 2007. Initial soil moisture retrieval from the METOP-A Advanced Scatterometer (ASCAT). Geogr. Res. Lett. 34, L20401.

Bogena, H.R., Huisman, J.A., Baatz, R., Franssen, H.-J.H., Vereecken, H., 2013. Accuracy of the cosmic-ray soil water content probe in humid forest ecosystems: the worst case scenario. Water Resour. Res. 49, 5778–5791.

Brocca, L., Hasenauer, S., Lacava, T., Melone, F., Moramacrco, T., Wagner, W., Dorigo, W., Matgen, P., Martinez-Fernandez, J., Llorens, P., Latron, J., Martin, C., Bittelli, M., 2011. Soil moisture estimation through ASCAT and AMSR-E sensors: an intercomparison and validation study across Europe. Remote Sens. Environ. 115, 3390–3408.

Cammalleri, C., Micale, F., Vogt, J., 2016. A novel soil moisture-based drought severity index (DSI) combining water deficit magnitude and frequency. Hydrol. Process. 30 (2), 289–301.

Carlson, T.N., Gillies, R.R., Perry, E.M., 1994. A method to make use of thermal infrared temperature and NDVI measurements to infer surface soil water content and fractional vegetation cover. Remote Sens. Rev. 9 (1–2), 161–173.

Carrao, H., Russo, S., Sepulcre-Canto, G., Barbosa, P., 2016. An empirical standardized soil moisture index for agricultural drought assessment from remotely sensed data. Int. J. Appl. Earth Obs. Geoinf. 48, 74–84.

Chakrabarti, S., Bongiovanni, T., Judge, J., Zotarelli, L., Bayer, C., 2014. Assimilation of SMOS soil moisture for quantifying drought impacts on crop yield in agricultural regions. IEEE J. Sel. Topics Appl. Earth Observ. Remote Sens. 7 (9), 3867–3879.

Chapin, E., Chau, A., Chen, J., Heavey, B., Hensley, S., Lou, Y., Machuzak, R., Moghaddam, M., 2012. AirMOSS: an airborne P-band SAR to measure root-zone soil moisture. Proc. IEEE Radar Conference. Atlanta, GA, pp. 693–698.

Crow, W., Koster, R., Reichle, R., Sharif, H., 2005. Relevance of time-varying and time-invariant retrieval error sources on the utility of spaceborne soil moisture products. Geophys. Res. Lett. 32, L24405. http://dx.doi.org/10.1029/2005GL024889.

Desilets, D., Zreda, M., 2013. Footprint diameter for a cosmic-ray soil moisture probe: theory and Monte Carlo simulations. Water Resour. Res. http://dx.doi.org/10.1002/wrcr.20187.

Djamai, N., Magagi, R., Goita, K., Hosseini, M., Cosh, M.H., Berg, A., Toth, B., 2015. Evaluation of SMOS soil moisture products over the CanEx-SM10 area. J. Hydrol. 520, 254–267.

Entekhabi, D., Njoku, E.G., O'Neill, P.E., Kellogg, K.H., Crow, W.T., Edelstein, W.N., Entin, J.K., Goodman, S.D., Jackson, T.J., Johnson, J., Kimball, J., 2010. The soil moisture active passive (SMAP) mission. Proc. IEEE 98 (5), 704–716.

Evans, J.G., Ward, H.C., Blake, J.R., Hewitt, E.J., Morrison, R., Fry, M., et al., 2016. Soil water content in southern England derived from a cosmic-ray soil moisture observing system: COSMOS-UK. Hydrol. Process. 30, 4987–4999.

Escorihuela, M.J., Chanzy, A., Wigneron, J.P., Kerr, Y.H., 2010. Effective soil moisture sampling depth of L-band radiometry: a case study. Remote Sens. Environ. 114, 995–1001.

Fascetti, F., Pierdicca, N., Pulvirenti, L., Crapolicchio, R., Munoz-Sabater, J., 2016. A comparison of ASCAT and SMOS soil moisture retrievals over Europe and Northern Africa from 2010 to 2013. Int. J. Appl. Earth Obs. Geoinf. 45, 135–142.

Fernandez-Moran, R., Al-Yaari, A., Mialon, A., Mahmoodi, A., Al Bitar, A., De Lannoy, G., Rodriguez-Fernandez, N., Lopez-Baeza, E., Kerr, Y., Wigneron, J.P., 2017. SMOS-IC: an alternative SMOS soil moisture and vegetation optical depth product. Remote Sens. 9, 457.

Franz, T.E., Zreda, M., Rosolem, R., Ferre, T.P.A., 2012. Field validation of a cosmic-ray neutron sensor using a distributed sensor network. Vadose Zone J. 11 (4).

Franz, T.E., Zreda, M., Rosolem, R., Ferré, T.P.A., 2013. A universal calibration function for determination of soil moisture with cosmic-ray neutrons. Hydrol. Earth Syst. Sci. 17, 453–460.

van Genuchten, M.Th., 1980. A closed-form equation for predicting the hydraulic conductivity of unsaturated soils. Soil Sci. Soc. Am. J. 44, 892–898.

U.S. Geological Survey, 1986. Hydrologic events and surface-water resources in National Water Summary. In: U.S. Geological Survey Water-Supply Paper 2300.

Gillies, R.R., Carlson, T.N., 1995. Thermal remote sensing of surface soil water content with partial vegetation cover for incorporation into climate models. J. Appl. Meteorol. 34, 745–756.

Hawdon, A., McJannet, D., Wallace, J., 2014. Calibration and correction procedures for cosmic-ray neutron soil moisture probes located across Australia. Water Resour. Res. 50, 5029–5043.

Hirschi, M., Mueller, B., Dorigo, W., Seneviratne, S.I., 2014. Using remotely sensed soil moisture for land–atmosphere coupling diagnostics: the role of surface vs. root-zone soil moisture variability. Remote Sens. Environ. 154, 246–252.

Hallikainen, M.T., Ulaby, F.T., Dobson, M.C., El-Rayes, M.A., 1985. Microwave dielectric behavior of wet soil—part 1: empirical models and experimental observations. IEEE Trans. Geosci. Remote Sens. 23 (1), 25–34.

Hogg, E.H., Hurdle, P.A., 1995. The aspen parkland in western Canada: a dry-climate analogue for the future boreal forest? Water Air Soil Pollut. 82, 391–400.

Huete, A., 1988. A soil adjusted vegetation index (SAVI). Remote Sens. Environ. 25 (3), 295–309. http://dx.doi.org/10.1016/0034-4257(88)90106-X.

Kabat, P., Beekma, J., 1994. Water in the unsaturated zone. In: Ritzema, H.P. (Ed.), Drainage Principles and Applications, Second ed. ILRI Publication 16. International Institute for Land Reclamation and Improvement, Wageningen, The Netherlands, pp. 383–434.

Keefer, T.O., Moran, M.S., Paige, G.B., 2008. Long-term meteorological and soil hydrology database, Walnut Gulch Experimental Watershed, Arizona, United States. Water Resour. Res. 44 (5), W05S07.

Kerr, H., Waldteufel, P., Wigneron, J.P., Martinuzzi, J., Font, J., Berger, M., 2001. Soil moisture retrieval from space: the Soil Moisture and Ocean Salinity (SMOS) mission. IEEE Trans. Geosci. Remote Sens. 39, 1729–1735.

Kohli, M., Schron, M., Zreda, M., Schmidt, U., Dietrich, P., Zacharias, S., 2015. Footprint characteristics revised for field-scale soil moisture monitoring with cosmic-ray neutrons. Water Resour. Res. 51 (7), 5772–5790.

Koster, R.D., Guo, Z., Yang, R., Dirmeyer, P.A., Mitchell, K., Puma, M., 2009. On the nature of soil moisture in land surface models. J. Clim. 22, 4322–4335.

Kumar, S.V., Reichle, R.H., Harrison, K.W., Peters-Lidard, C.D., Yatheendradas, S., Santanello, J.A., 2012. A comparison of methods for a priori bias correction in soil moisture data assimilation. Water Resour. Res. 48, W03515.

Liu, H.Q., Huete, A., 1995. A feedback based modification of the NDVI to minimize canopy background and atmospheric noise. IEEE Trans. Geosci. Remote Sens. 33 (2), 457–465.

Liu, D., Mishra, A.K., Yu, Z.B., Yang, C.G., Konapala, G., Vu, T., 2017. Performance of SMAP, AMSR-E and LAI for weekly agricultural drought forecasting over continental United States. J. Hydrol. 555, 88–104.

Lv, L., Franz, T.E., Robinson, D.A., Jones, S.B., 2014. Measured and modeled soil moisture compared with cosmic-ray neutron probe estimates in a mixed forest. Vadose Zone J. 13 (12). http://dx.doi.org/10.2136/vzj2014.06.0077.

Martinez-Fernandez, J., Gonzalez-Zamora, A., Sanchez, N., Gumuzzio, A., 2015. A soil water based index as a suitable agricultural drought indicator. J. Hydrol. 522, 265–273.

Martinez-Fernandez, J., Gonzalez-Zamora, A., Sanchez, N., Gumuzzio, A., Herrero-Jimenez, C.M., 2016. Satellite soil moisture for agricultural drought monitoring: assessment of the SMOS derived Soil Water Deficit Index. Remote Sens. Environ. 177, 277–286.

Mattikalli, N.M., Engman, E.T., Jackson, T.J., Ahuja, L.R., 1998. Microwave remote sensing of temporal variations of brightness temperature and near surface soil water content during a watershed-scale field experiment, and its application to the estimation of soil physical properties. Water Resour. Res. 34, 2289–2299.

McKee, T.B., Doesken, N.J., Kleist, J., 1993. The relationship of drought frequency and duration to time scales. In: Proceedings of the Eighth Conference on Applied Climatology. American Meteorological Society, Boston, pp. 179–184.
McPherson, R.A., Fiebrich, C.A., Crawford, K.C., Kilby, J.R., Grimsley, D.L., Martinez, J.E., Basara, J.B., Illston, B.G., Morris, D.A., Kloesel, K.A., Melvin, A.D., 2007. Statewide monitoring of the mesoscale environment: a technical update on the Oklahoma Mesonet. J. Atmos. Ocean. Technol. 24 (3), 301–321.
Merlin, O., Rüdiger, C., Al Bitar, A., Richaume, P., Walker, J., Kerr, Y., 2012. Disaggregation of SMOS soil moisture in southeastern Australia. IEEE Trans. Geosci. Remote Sens. 99, 1–16.
Mironov, V.L., Kosolapova, L.G., Fomin, S.V., 2009. Physically and mineralogically based spectroscopic dielectric model for moist soils. IEEE Trans. Geosci. Remote Sens. 47, 2059–2070.
Mishra, A., Vu, T., Veetti, A.V., Entekhabi, D., 2017. Drought monitoring with soil moisture active passive (SMAP) measurements. J. Hydrol. 552.
Montzka, C., Bogena, H.R., Zreda, M., Monerris, A., Morrison, R., Muddu, S., Verrecken, H., 2017. Validation of spaceborne and modelled surface soil moisture products with cosmic-ray neutron probes. Remote Sens. 9, 103.
Nachtergaele, F.O., van Velthuizen, H.T., Verelst, L., Wiberg, D., Batjes, N.H., Dijkshoorn, J.A., van Engelen, V.W.P., Fischer, G., Jones, A., Montanarella, L., et al., 2012. Harmonized World Soil Database (Version 1.2). FAO, Rome, Italy, IIASA, Laxenburg, Austria.
Naeimi, V., Scipal, K., Bartalis, Z., Hasenauer, S., Wagner, W., 2009. An improved soil moisture retrieval algorithm for ERS and METOP scatterometer observations. IEEE Trans. Geosci. Remote Sens. 47, 1999–2013.
Owen, T.W., Carlson, T.N., Gillies, R.R., 1998. An assessment of satellite remotely-sensed land cover parameters in quantitatively describing the climatic effect of urbanization. Int. J. Remote Sens. 19, 1663–1681.
Palmer, W.C., 1965. Meteorological drought. In: U.S. Weather Research Paper 45 U.S. Weather Bureau, Washington D.C..
Peng, J., Niesel, J., Loew, A., Zhang, S., Wang, J., 2015. Evaluation of satellite and re-analysis soil moisture products over Southwest China using ground-based measurements. Remote Sens. 7, 15729–15747.
Piles, M., Sánchez, N., Vall-llossera, M., Camps, A., Martínez-Fernández, J., Martinez, J., Gonzalez-Gambau, V., 2014. A downscaling approach for SMOS land observations: evaluation of high-resolution soil moisture maps over the Iberian peninsula. IEEE J. Sel. Topics Appl. Earth Observ. Remote Sens. 7 (9), 3845–3857.
Palmer, W.C., 1968. Keeping track of crop moisture conditions, nationwide: the new crop moisture index. Weatherwise 21 (4), 156–161.
Rahimzadeh-Bajgiran, P., Berg, A.A., Champagne, C., Omasa, K., 2013. Estimation of soil moisture using optical/thermal infrared remote sensing in the Canadian Prairies. ISPRS J. Photogramm. Remote Sens. 83, 94–103.
Reichle, R.H., Koster, R.D., 2004. Bias reduction in short records of satellite soil moisture. Geogr. Res. Lett. 31, L19501.
Renard, K.G., Lane, L.J., Simanton, J.R., Emmerich, W.E., Stone, J.J., Weltz, M.A., Goodrich, D.C., Yakowitz, D.S., 1993. Agricultural impacts in an arid environment: Walnut Gulch studies. Hydrol. Sci. Technol. 9 (1–4), 145–190.
Rim, C.S., 2000. A comparison of approaches for evapotranspiration estimation. KSCE J. Civ. Eng. 4 (1), 47–52.
Robinson, D.A., Campbell, C.S., Hopmans, J.W., Hornbuckle, B.K., Jones, S.B., Knight, R., Ogden, F., Selker, J., Wendroth, O., 2008. Soil moisture measurement for ecological and hydrological watershed-scale observatories: a review. Vadose Zone J. 7 (1), 358–389. http://dx.doi.org/10.2136/vzj2007.0143.
Rosolem, R., Shuttleworth, W.J., Zreda, M., Franz, T.E., Zeng, X., Kurc, S.A., 2013. The effect of atmospheric water vapor on neutron count in the cosmic-ray soil moisture observing system. J. Hydrometeorol. 14, 1659–1671.
Rötzer, K., Montzka, C., Bogena, H., Wagner, W., Kerr, Y., Kidd, R., Vereecken, H., 2014. Catchment scale validation of SMOS and ASCAT soil moisture products using hydrological modeling and temporal stability analysis. J. Hydrol. 519, 934–946.
Sadeghi, M., Jones, S.B., Philpot, W.D., 2015. A linear physically-based model for remote sensing of soil moisture using short wave infrared bands. Remote Sens. Environ. 164, 66–76.
Sadeghi, M., Babaeian, E., Tuller, M., Jones, S.B., 2017. The optical trapezoid model: a novel approach to remote sensing of soil moisture applied to Sentinel-2 and Landsat-8 observations. Remote Sens. Environ. 198, 52–68.
Santos, W.J.R., Silva, B.M., Oliveira, G.C., Volpato, M.M.L., Lima, J.M., Curi, N., Marques, J.J., 2014. Soil moisture in the root zone and its relation to plant vigor assessed by remote sensing at management scale. Geoderma 221, 91–95.
Schaap, M.G., Leij, F.J., van Genuchten, M.T., 2001. ROSETTA: a computer program for estimating soil hydraulic parameters with hierarchical pedotransfer functions. J. Hydrol. 251 (3–4), 163–176.
Shafian, S., Maas, S.J., 2015. Improvement of the Trapezoid method using raw Landsat image digital count data for soil moisture estimation in the Texas (USA) High Plains. Sensors 15 (1), 1925–1944.
Sohrabi, M.M., Ryu, J.H., Abatzoglou, J., Tracy, J., 2015. Development of soil moisture drought index to characterize droughts. J. Hydrol. Eng. 20 (11), 04015025.
Sridhar, V., Hubbard, K.G., You, J., Hunt, E.D., 2008. Development of the soil moisture index to quantify agricultural drought and its "user friendliness" in severity-area-duration assessment. J. Hydrometeorol. 9 (4), 660–676.
Sun, H., 2016. Two-stage trapezoid: a new interpretation of the land surface temperature and fractional vegetation coverage space. IEEE J. Sel. Topics Appl. Earth Observ. Remote Sens. 9 (1), 336–346.
Tabatabaeenejad, A., Burgin, M., Duan, X., Moghaddam, M., 2015. P-band radar retrieval of subsurface soil moisture profile as a second-order polynomial: first AirMOSS results. IEEE Trans. Geosci. Remote Sens. 53 (2), 645–658.
Thornthwaite, C.W., 1948. An approach towards a rational classification of climate. Geogr. Rev. 38, 55–94.
Torres-Ruiz, J.M., Diaz-Espejo, A., Morales-Sillero, A., Martín-Palomo, M.J., Mayr, S., Beikircher, B., Fernández, J.E., 2013. Shoot hydraulic characteristics, plant water status and stomatal response in olive trees under different soil water conditions. Plant Soil 373 (1–2), 77–87.
Van der Schalie, R., Kerr, Y.H., Wigneron, J.P., Rodríguez-Fernández, N.J., Al-Yaari, A., de Jeu, R.A.M., 2016. Global SMOS soil moisture retrievals from the land parameter retrieval model. Int. J. Appl. Earth Obs. Geoinf. 45, 125–134.
Vereecken, H., Huisman, J.A., Pachepsky, Y., Montzka, C., van der Kruk, J., Bogena, H., Weihermüller, L., Herbst, M., Martinez, G., Vanderborght, J., 2014. On the spatio-temporal dynamics of soil moisture at the field scale. J. Hydrol. 516, 76–96.
Wagner, W., Hahn, S., Kidd, R., Melzer, T., Bartalis, Z., Hasenauer, S., Figa-Saldana, J., de Rosnay, P., Jann, A., Schneider, S., Komma, J., 2013. The ASCAT soil moisture product: a review of its specifications, validation results and emerging applications. Meteorol. Z. 22, 5–23.
Wigneron, J.P., Kerr, Y., Waldteufel, P., Saleh, K., Escorihuela, M.J., Richaume, P., Ferrazzoli, P., de Rosnay, P., Gurney, R., Calvet, J.C., et al., 2007. L-band microwave emission of the biosphere (L-MEB) model: description and calibration against experimental data sets over crop fields. Remote Sens. Environ. 107, 639–655.
Wigneron, J.P., Schwank, M., Baeza, E.L., Keer, Y., Novello, N., Millan, C., Moisy, C., Richaume, P., Mialon, A., Al Bitar, A., et al., 2012. First evaluation of the simultaneous SMOS and ELBARA-II observations in the Mediterranean region. Remote Sens. Environ. 124, 26–37.
Zhang, F., Zhang, L., Wang, X., Hung, J., 2013. Detecting agro-droughts in southwest of China using MODIS satellite data. J. Integr. Agric. 12 (1), 159–168.
Zreda, M., Desilets, D., Ferre, T.P.A., Scott, R.L., 2008. Measuring soil moisture content non-invasively at intermediate spatial scale using cosmic-ray neutrons. Geogr. Res. Lett. 35, L21402.
Zreda, M., Shuttleworth, W.J., Zeng, X., Zweck, C., Desilets, D., Franz, T., Rosolem, R., 2012. COSMOS: the cosmic-ray soil moisture observation system. Hydrol. Earth Syst. Sci. 16, 4079–4099.